NASA CR-168352

CONTRACT NAS5-25727
VERY HIGH RESOLUTION UV AND X-RAY
SPECTROSCOPY AND IMAGERY OF
SOLAR ACTIVE REGIONS
FINAL REPORT

(NASA-CR-168352) VERY HIGH RESOLUTION UV AND X-RAY SPECTROSCOPY AND IMAGERY OF SOLAR ACTIVE REGIONS Final Report (Lockheed Missiles and Space Co.) 63 p Avail: NTIS HC A04/MF A01

N87-30243

Unclas
CSCL 03B G3/92 0100137

Lockheed Missiles & Space Company, Inc.
SUNNYVALE, CALIFORNIA

CONTRACT NAS5-25727
VERY HIGH RESOLUTION UV AND X-RAY SPECTROSCOPY AND IMAGERY OF SOLAR ACTIVE REGIONS
FINAL REPORT

D#068438

VERY HIGH RESOLUTION UV AND X-RAY SPECTROSCOPY AND IMAGERY OF SOLAR ACTIVE REGIONS

FINAL REPORT

JULY 1987

M.E.C. Bruner	Principal Investigator
W.A. Brown	Program Scientist
L.W. Acton	Co-Investigator
R.C. Catura	Co-Investigator
B.M. Haisch	Co-Investigator
C.J. Wolfson	Co-Investigator

Lockheed Palo Alto Research Laboratory
Department 91-20, Building 255
3251 Hanover Street
Palo Alto, California 94304

J.H. Underwood — Co-Investigator

Center for X-Ray Optics at
Lawrence Berkeley Laboratory
Berkeley, California 94720

Scientific Collaborators Outside the U.S.A.

R.M. Bonnet

European Space Agency
8-10 Rue Mario Nikis
75738 Paris Cedex
Paris, France

L. Dame

Lab. de Physique Stellaire et Planetaire, CNR
91370 Verrieres le Buisson
Paris, France

CONTRACT NAS5-25727
FINAL REPORT

Table of Contents

FIGURE 1

CONTRACT NAS5-25727
FINAL REPORT

1.0 Overview

The broad objective of this research program has been to investigate the properties of plasmas in the atmosphere of the Sun and from them, to infer the physical conditions and processes in the observed regions. This report is the last in a series covering seven years of the Solar Rocket Program at Lockheed Research Laboratory in the Space Astronomy Group. It highlights new results in high resolution soft x-ray spectroscopy and plasma diagnostics of the solar corona and UV imagery in the chromosphere-corona transition region.

Our basic tools in this investigation have been high resolution spectroscopy in the soft X-ray region, and high resolution narrow band imaging in the ultraviolet. The primary data have been collected during a series of four sounding rocket flights. The last three flights of the series were conducted under this contract; the first flight was supported under an earlier contract, and the resulting data were considered as part of the analysis effort on this contract. Rocket flight data have been augmented in each case with data from ground based observatories and from satellites. From the outset, the relationship between the solar plasmas in the corona and transition region and the chromospere was sought by incorporating in the rocket payload instruments sensitive to radiation in spectral bands and lines originating in temperature regimes characteristic of a cross section of altitudes in the solar atmosphere.

Hardware used for the investigation included a high resolution X-ray spectrograph developed under the previous contract and several new instrument components developed under this contract. The French team at LPSP in Verrieres-le-Buisson, with CNES support, contributed the very successful TRC (transition Region Camera) to the payload's instrument complement. This 10 cm diameter Cassegrain telescope with narrow band UV filters and photographic detection produced sub-arc second images of the sun in Lyman Alpha and in the 1600A interval. A new normal incidence x-ray telescope provided a solar soft-x-ray image at 44 Angstroms from a 30 second exposure with a 1.5 inch diameter objective. New developments in design of other advanced space hardware were initiated in imaging photoelectric spectral detectors and, in France, Fabry-Perot Tunable filters for the UV. Building on the unique focus-by-metrology technology developed in earlier NASA work (under NAS2-9181) these experiments, and the laboratory work and data analysis supporting them, broke new ground in solar spectroscopy. The unique international flavor of the team participating in the program has, and will continue to, contribute to its success.

A summary of the work done during the program is given in section 2 of this report. A more extended discussion is given in section 3.

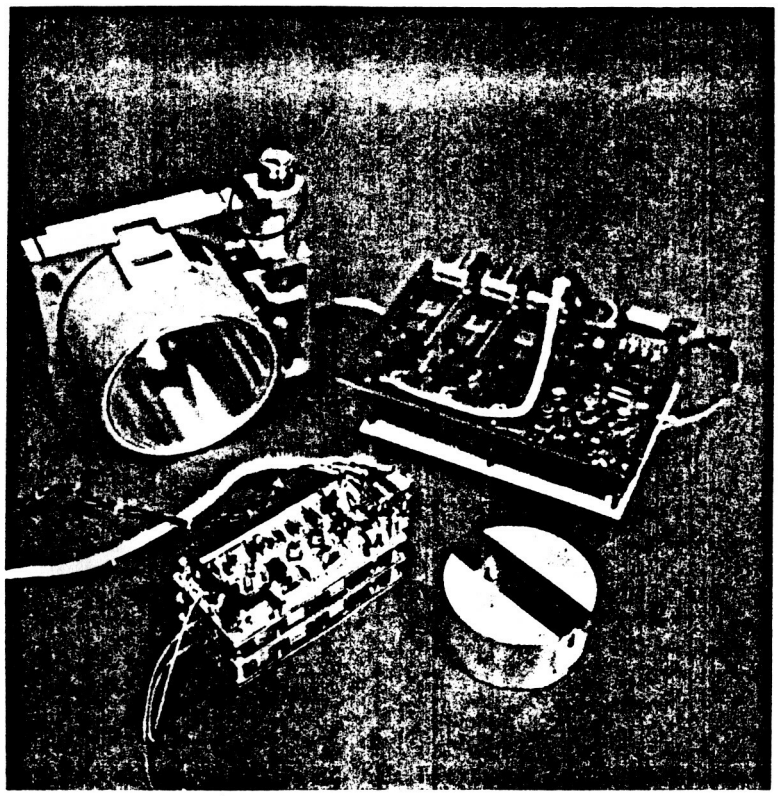

FIGURE 2

2.0 Program Highlights

The work that has been done in support of this contract may be divided into four general categories, hardware development, sounding rocket flights, the program of scientific analysis of the resulting data, and the initial planning phase for a follow-on program based on the SPARTAN system. A brief synopsis of these efforts is given in this section.

2.1 Hardware Development

The contract began with an initial inventory of flight hardware that had been developed under contract NAS2-9181. This consisted primarily of a sounding rocket payload, its ground support equipment, and associated test fixtures. The payload included the X-ray Spectrograph / Spectrometer Telescope system, (XSST), an H-alpha telescope and filtergraph system, the Transition Region Camera (TRC, an instrument defined in collaboration with the Labroatoire de Physique Stellaire et Planetaire and developed by them), and a structural and thermal control system. The XSST included a parabolic collecting mirror and cell, a curved optical bench, a slit assembly, a grating assembly, a central image detector, and a detector system consisting of a plateholder and a series of discrete photoelectric detectors.

Hardware developed and flown during the performance of the contract included a roll film spectrograph camera, an X-ray sensitive central image detector, and a normal incidence soft X-ray imaging system. In addition, hardware development work was carried out on a position sensitive soft X-ray camera for the spectrograph, a normal incidence soft X-ray turret camera, and a structural test panel for possible use in the SPARTAN program.

2.2 Sounding Rocket Flights

Three sounding rocket flights were carried out during the course of the program. In the first flight, our goals were to record the soft X-ray spectrum of a solar active region, to photograph the region in the UV with sub-arc-second spatial resolution, and to gather supporting observations from ground based observatories and from the SMM satellite. The plateholder for the X-ray spectrograph had been modified to make it more tolerant of high voltage corona discharges that had been observed during the first flight. In spite of these modifications, the high voltage was inadvertently turned on due to an electrical anomaly late in the flight, and the plate was fogged beyond use. The UV experiment, however, was quite successful as was the program of supporting observations.

For the second flight, we developed a roll film camera to replace the plateholder / photoelectric detector system of the XSST. This modification was made both to assure the

survivability of the photographic image, and to make the system suitable for the long term flight opportunities that were being actively discussed within NASA. We were extremely fortunate during the second flight to observe a solar flare at the time of soft X-ray maximum. The resulting spectrum contained over 400 lines in the 10 to 95 Angstrom range. The UV camera again produced an excellent series of images. Both data sets have been extensively analyzed, and a number of papers have been published or are in preparation.

The third flight was to have been carried out in a joint observing program with the Spacelab 2 mission, the major focus of the science being the detailed comparison of magnetograph data from the SOUP experiment with the high resolution images from the UV camera. The X-ray spectrograph was to have played a supporting role. Newly developed for this flight was a demonstration experiment to use normal incidence multi-layer mirror technology to make narrow band images of soft X-ray coronal loops. Development work on the X-ray position sensitive detector could not be completed in time for the Spacelab 2 launch in the summer of 1985. The planned joint observing with Spacelab 2 could not be done because of a frustrating series of problems with both the rocket hardware (which was damaged by lightning during a severe thunderstorm) and with the SOUP instrument. The flight was finally carried out in the fall, using ground based instruments to make the observations originally planned for SOUP.

2.3 Science Program

Both the UV filtergraph and the X-ray spectrograph have contributed significant bodies of new information about the sun's atmosphere. The 1980 flight data have been used in studies of the meso-granulation network and of electric currents associated with chromospheric structures. An expected correlation of currents derived from magnetograms with heated regions in the chromosphere and transition zone was not confirmed by the rocket data. The 1982 X-ray flare spectrum represents the most comprehensive set of solar observations extant in the 10 to 100 Angstrom range, and is being used for testing differential emission measure analysis techniques. The spectrum has been carefully classified, and the published line list now serves as the reference standard for this region of the spectrum. A number of new density diagnostic line ratios have been identified in the spectrum, and new atomic physics calculations have been done for use in their interpretation. The density determinations have been combined with the differential emission measure analysis to derive the temperature distribution of emitting volume. The density determinations have also shown that the different temperature regions cannot be in hydrostatic equilibrium, and that the magnetic field must play an important role in the pressure balance. A model based on a shell geometry has been advanced to interpret the observations.

The 1985 data confirmed the suspected correlation between

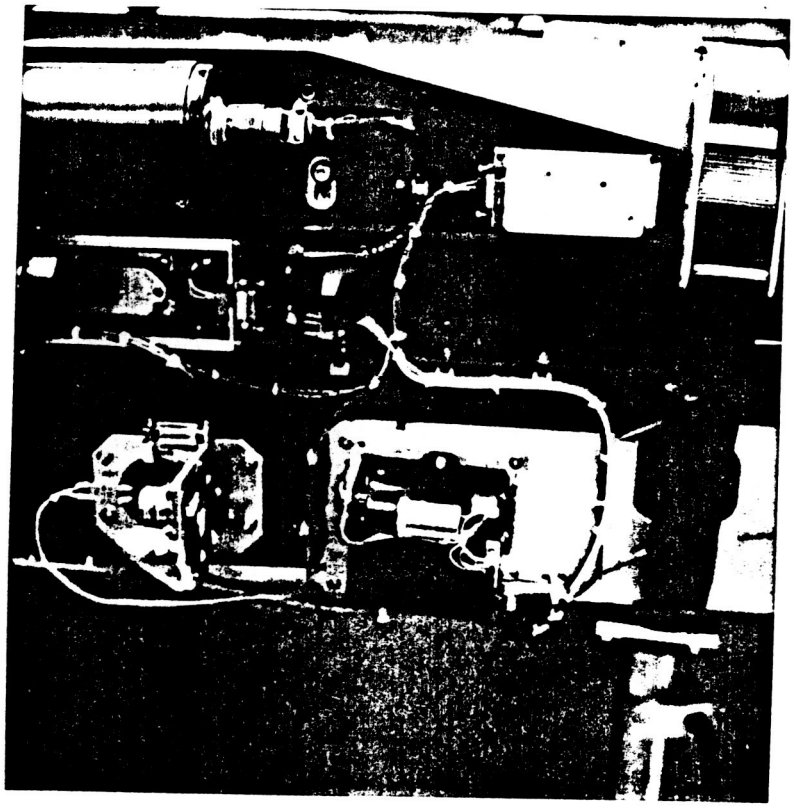

FIGURE 3

the 1600 continuum cell bright point system (discovered in the 1979 flight data) and the Ca II v bright point system. High resolution magnetograms made from the ground during the flight are expected to confirm the predicted correlation between these two systems and local concentrations in the vertical component of the magnetic field. The normal incidence X-ray camera was successful in recording 44 Angstrom images of a system of coronal loops over an active region. This was the first successful use of multilayer mirror technology for astronomical observations. Analysis of the X-ray spectrum showed that the loop system had an emission measure distribution that was intermediate between that of a typical active region and of a flare, suggesting that the plasma represented cooling material from a flare that had taken place earlier in the day.

2.4 SPARTAN Initial Planning

In response to a NASA Dear Colleague letter, we submitted in July of 1984 our proposal LMSC-D088449 in which we recommended the conversion of this sounding rocket program into a SPARTAN investigation that would be flown on a Shuttle mission. The proposal was favorably reviewed, and was selected by NASA as one of several SPARTAN investigations. Accordingly, we began an SPARTAN accommodation study, developed preliminary structural and electrical system concepts, and participated in a pre-PIC (project initiation conference) held at GSFC. As part of the study, we invented a concept for a light weight all-metal optical table, and prepared a test panel for evaluation. Unfortunately, the Challenger disaster and its aftermath has severely restricted access to space via the Space Transportation System and it appears that the SPARTAN launch opportunity has been indefinitely delayed or lost.

3.0 Program Activities

3.1 Hardware Development Work

The content of this section has been compiled from various reports and other documents developed during the course of the contract. The text has been edited where appropriate, and a few explanatory notes have been added.

3.1.1 Roll Film Camera

The original detector system for the XSST combined both photographic and photoelectric detectors within a single enclosure in order to allow spectrum mapping and multiple line photometry to be done with the same unit. A roll film camera was developed for the X-ray spectrograph to replace the original detector system, both to eliminate the recurrence of corona discharge and plate fogging problems that were encountered in the first two flights, and to allow us to make multiple spectrograms during a flight. A considerable amount of effort went into the design, fabrication and testing of this camera, which is unique in satisfying the following requirements:

1. It provides several exposures without fogging (by pressure, electrical discharge, or abrasion) the extremely delicate UV emulsions of Eastman Kodak's 101 series.

2. It holds the film accurately on the 5 meter diameter Rowland circle of the spectrograph, yet has the capability to be removed to a darkroom for reloading.

3. It hermetically seals the film so that accidental breakdown of high voltage electronic detectors cannot endanger the experiment.

These requirements were met by a clever mechanical design and a new micro processor controlled electromechanical system which advances the film, moves the pressure plate and opens and closes the sealing door in flight. A photograph of the completed camera assembly is shown in Figure 1.

Laboratory tests of the completed camera in the fall of 1981 validated the mechanical and electronic systems and it was used during the July, 1982 and Oct., 1985 flights.

3.1.2 Central Image Detector Modifications

After flight 27.036 it was decided to develop and replace the XSST plate holder and Spiraltron assembly with the roll film camera described above. Since this camera has no photoelectric detectors to provide real time telemetry of solar X-ray fluxes in flight, it would be difficult or impossible to point the narrow field of view of the XSST at the bright X-ray features in solar active regions. To overcome this deficiency an X-ray central image detector was added to the existing UV central image detector. The UV detector has proven useful in previous flights in detecting the solar limb and thereby providing the corrections to the aspect solution obtained from the video and film H-alpha camera data. The X-ray new central image detector also has the important role of allowing the instrument to be pointed at a point-like X-ray source in the laboratory. Use of a Spiraltron electron multiplier as the X-ray central image monitor was dictated by space and weight limitations. The new hermetically sealed film camera, together with a high voltage camera door interlock gave sufficient protection from plate fogging encountered with the earlier design.

3.1.3 Position Sensitive X-ray Detector

A major hardware effort was the design and development of a position sensitive photon counting detector for use in the X-ray spectrograph. This was sized to cover the XSST spectrum between 30 and 40 Angstroms and allows the film camera to be placed on the curved optical bench behind it to record longer wavelengths in first order and the second order spectra of some shorter wavelengths. This detector uses microchannel plates in a Z configuration to detect and amplify X-ray photons, producing an electronic

image. We use a wedge and strip anode assembly, following the general design developed at the Space Science Laboratory in Berkeley. The new detector is expected to be about an order of magnitude more sensitive than the film permitting us to record useful spectra of much fainter sources.

Highlights of the detector development program include the following:

- Receipt of a 600 mm dia. microchannel "Z" plate assembly from Galileo.
- Completion of fabrication of the detector electronics system and the beginning of subsystem testing. Components completed include the pulse amplifiers, the ADC system, the PCM interface system, and the GSE interface system.
- Completion of the design for the position sensitive detector system test chamber and the procurement of parts from corporate fixed assets.
- Completion of most of the mechanical design for the detector. Fabrication of the auxiliary vacuum compartment, detector base, actuator mechanism and related mechanical parts.

Work on the position sensitive detector for the X-ray spectrograph proceeded to the point where all of the major components had been received or fabricated. The mechanical components of the detector assembly were completed and partly assembled. Subsystem testing of the amplifiers and of the digital electronics is complete. A baseline test software package running on an LSI-11 computer was completed, and used for verification of the digital pulse processing electronics. The unit is essentially ready for assembly and functional testing. The equipment is illustrated in Figure 2. Completion of the detector required more time and effort than we had hoped, however, and we considered the schedule risk to be sufficiently high that its use for the coordinated experiment with Spacelab 2 was unwise. Accordingly, we suspended the detector development program in order to devote our resources to the coordinated experiment with Spacelab 2. The hardware is being preserved for use in the next phases of this investigation.

3.1.4 Normal Incidence X-ray Imaging System

This unique device provided the first normal incidence x-ray image of the sun. It consists of a one-element telescope of 1 meter focal length, a camera assembly and a shutter assembly. The multilayer X-ray mirror was prepared by the Energy Conversion Devices Corporation using a design by Dr. J. Underwood of the Lawrence Berkeley Laboratory, our co-investigator on this part of the program. Using a sputtering technique, 30 tungsten-carbon layer pairs (nominally 7.65 A of W and 14.5 A of C) were deposited on a 4 cm diameter spherical mirror having a 2 m concave

radius of curvature.

The mirror was designed to observe the strong Si XII line at 44.16 A, just on the long wavelength side of the carbon K absorption edge (43.68 A); this considerably simplified the filtering out of shorter wavelength X-ray lines reflected in higher orders, and extreme ultraviolet and ultraviolet contamination at longer wavelengths. The multilayer d-spacing was measured to be 21.934 A based on the angular reflection peak of a monochromatic beam. The mirror was designed to have a relatively broad band, hence a moderate peak reflectivity, R = 0.025. The peak wavelength of 43.87 A achieved the design requirement; the absolute value of R has not yet been verified experimentally.

The mirror was attached to the central payload spar and tilted by 1.7 degrees to the line-of-sight, allowing direct, off-axis imaging at the Herschelian focus 100 cm away, yielding a solar image approx. 1 cm in diameter in the focal plane. The image was recorded on Kodak SO-212 film in a camera developed for an earlier rocket flight. Eight pieces of film, each with its own individual light-excluding filter, were mounted on a turret inside a camera equipped with an electrically operated dark slide and shutter. The turret was rotated by a clockwork mechanism during the flight to make the exposures. Figure 3 shows the camera and shutter assembly mounted on the instrument spar. The film, left over from the SKYLAB mission, is sensitive to 40--60 A X-rays. Double 1 micron thick polypropylene filters each with a 1000 A aluminum coating were placed directly in front of each of the eight film pieces to exclude visible and ultraviolet light.

3.1.5 SPARTAN Planning

The SPARTAN concept was a very exciting one for our investigation, because of the possibility for making extended observations. This would permit the use of very long exposures with the X-ray spectrograph, enabling us to exploit the full diagnostic potential of the soft X-ray region on the quiet corona, and on active region loops. It would also have allowed us to observe the evolution of structures visible both in X-rays and in the ultraviolet, giving us a powerful new tool for studying the dynamics of the transition zone and corona.

Planning for the SPARTAN included supporting a preliminary Project Initiation Conference (PIC) at GSFC. A data package prepared for this meeting is included as an appendix to this report. It describes both the command and data handling system for the payload, and a novel mechanical configuration discussed in the next section.

3.1.6 SPARTAN structural System

In order to adapt our rocket hardware to the SPARTAN, a new structural system was required, since the metering spar of the

XSST was a welded aluminum structure. Use of such a welded structure violated STS safety analysis requirements, and was prohibited. Since the SPARTAN carrier would be carried in the Shuttle cargo bay, we would not be restricted to the cylindrical geometry of a sounding rocket compartment, and could base our design on a rectangular cross section. This led us to develop a concept for a structural system based on a pair of optical tables joined together with a pair of optical benches. We call our concept the Spartan Optical Table System (SPOTS). The benches were to be made from standard aluminum extrusions to save cost. For the tables, we considered three approaches: a structure milled from solid plate, a dip-brazed composite structure consisting of aluminum foam with thin face sheets, and a furnace brazed composite structure consisting of alternate layers of thin corrugated aluminum. We wanted an all-metal system to minimize problems with outgassing. The aluminum foam concept was dropped due to the reluctance of the sole supplier to provide support for the project. A test panel of the furnace brazed composite was prepared showing that the process presented no special difficulties. Uncertainty over the direction of the program, brought about by the Challenger disaster, led us to take a cautious approach to proceeding with the detailed mechanical design work on the new structural support system. The test panel has been delivered and placed into the hardware inventory for future evaluation.

In 1986, the restructuring (loss) of flight opportunities for our payload led us to begin work on a composite optical table, sized for a 22 inch diameter rocket payload, and adaptable to an eventual satellite or space station observatory. In form, a two sided optical bench, it will allow precision mounting of the optical components of the SPARTAN instrument complement so that they can be flown on sounding rockets until such time as a long term flight opportunity becomes available. Thermal stability will be inherent in the carbon-epoxy structure. The present design has been the subject of an in-house numerical simulation of the vibrational resonances encountered when our instrument groups are mounted and the rocket bulkhead attachments are in place.

3.1.7 X-ray Turret Camera

The x-ray imaging system for the rocket was very simple, consisting of a multilayer coated normal incidence mirror, a shutter, a long wavelength rejection filter, and a film camera. The SPARTAN version will consist of four such mirrors mounted on a turret. The multilayer coating on each mirror will select a narrow portion of the soft x-ray spectrum thus imaging the plasma at the excitation temperature which emits the lines in the active bandwidth. The Si XII line at 44.16 A is one candidate chosen to be longward of the carbon absorption edge since the multilayer mirror coating will probably include carbon as the dielectric spacer.

Since the X-ray Turret Camera is a modular design, its design does not depend strongly on the form of the vehicle. In

light of the current program uncertainty, we decided (with the concurrence of Dr. Bohlin, our NASA Discipline Chief) to proceed with the development of the turret design in such a way that it could be flown in either a rocket or a SPARTAN payload. The mechanical design of the turret has been completed. Most of the parts of the turret assembly have been fabricated and assembled, and are available for the follow-on investigation. The partially assembled turret and a mirror cell are shown in Figure 4.

Images from the X-ray Turret Camera will be recorded on roll film. We intend to use a commercial 35 mm camera as a film transport and shutter mechanism. Our tentative selection for the camera is a Canon model T 70 (less lens). Tests at MSFC have shown that the T 70 model is capable of transporting Eastman Kodak type 101-01 perforated spectroscopic film without inducing either scratches or blemishes due to electrostatic discharge. The T 70 has an internal motor drive, and requires only a switch closure to operate. A unit has been procured for evaluation, and is part of the residual inventory.

3.2 Sounding Rocket Flight Program

This section will discuss the rocket flight activities in general, with an emphasis on the circumstances of each flight. The results of analysis of the flight data have been discussed in the open literature, in presentations at scientific meetings, and in papers that are being prepared for publication. A bibliography is given later in section 3.2.5.

3.2.1 Flight of 27.036 - 23 Sept., 1980

Launch and solar pointing operations for this flight were nearly perfect. This flight achieved most, but not all, of the scientific objectives. X-ray signals were recorded by the Spiraltron detectors in the XSST and an excellent sequence of UV solar images were recorded by the TRC in 1215 and 1600 A. The XSST spectrographic plate was fogged, probably late in the flight due to a spurious command signal which re-activated the high voltage to the electron multipliers after the pressure had risen.

This flight was supported by a concerted program of co-ordinated observations from the SMM spacecraft, which was fully functional, and from several ground based observatories. The data set collected was of unprecedented quality and completeness.

3.2.2 Flight of 27.054 - 13 July, 1982

There were several active regions present on the disk, the most notable being NOAA region 3804, which had produced a class X flare some hours before our scheduled launch. Also present was a new compact region, NOAA 3806, which we identified as a secondary target.

At about 1625 UT, we were notified by the observer at the Big Bear Solar Observatory that a flare was in progress in our

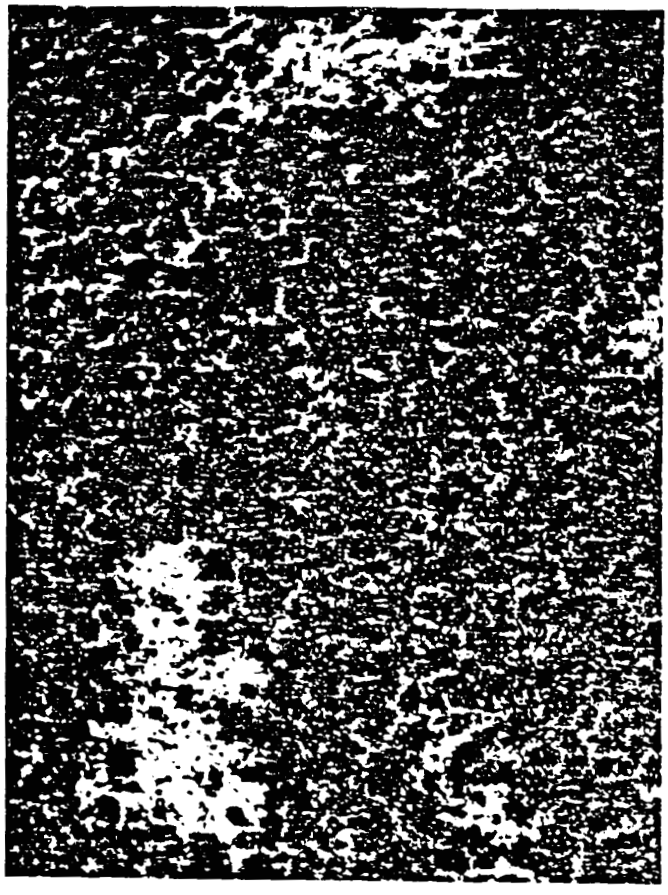

Figure 3

secondary target region. The flare was also evident in the GOES signal, which rose rapidly toward an eventual level of C-8. At this point we redefined our objective! The rocket was launched at 1630 UT as scheduled, and the SPARCS pointing system acquired the Sun about 80 seconds later.

Once Solar pointing had been established, the flare was identified on the H-Alpha television image, and the payload re-oriented by ground command to center the flare in the field of view. At this point, the automated bright point search routine was initiated. A spatial scan was performed by electronics contained in the flight package, while the signal levels from the UV and X-ray detectors in the spectrograph were monitored via telemetry by the ASCL computer in the control. At the end of the search phase, the computer identified the location of the brightest position seen by the X-ray detector, and formulated the commands necessary to re-orient the payload. The search was carried out in two phases; a coarse one in which a rectangular field of 160 x 100 arc sec was scanned and a fine one which covered a single line about 30 arc sec long. The pointing was adjusted between scans such that the fine scan was centered on the brightest location found in the coarse scan. The search sequences required a total of 45 sec for completion.

At the completion of the bright point search sequences, the shutter of the X-ray spectrograph was opened for the first of two planned exposures. The first exposure lasted about 50 sec, and the second about 140 sec. The film transport was commanded to advance between the two exposures, but failed to operate correctly. Instead, the film advanced only about 0.5 mm, leaving both exposures on the same segment of film. Fortunately, the motion was sufficient to separate the two sets of lines, so that micro-densitometry and analysis was still possible. During the time that the spectrum was being recorded, the ultraviolet filtergraph made a series of images in each of the defined wavelength bands.

At the end of data taking, the vacuum door was sealed so that the equipment re-entered the atmosphere in an evacuated state. Parachute recovery was nominal, and the payload was returned to the laboratory within about two hours in undamaged condition. Although some command anomalies were experienced, the quality of the flight data was not affected.

3.2.3 Flight of 27.090 - 25 Oct., 1985

The object of this flight was to make a coordinated study of small scale structure in weak magnetic fields, Ca II and the ultraviolet continuum. We had enlisted the aid of scientists at several major ground based observatories including Sacramento Peak, the Big Bear Solar Observatory, Kitt Peak Observatory, and the MSFC Solar Observatory.

The flight of Nike Black Brant V sounding rocket mission 27.090 was completely successful. The ultraviolet filtergraph,

which was our prime experiment on this flight, produced a wealth of images, all in focus and showing a great deal of fine structure. There are at least two prominence regions on the west limb that we will be able to study in addition to the disk fine structure that was our main objective. We got a faint, but quite usable X-ray spectrum showing lines from C VI to Fe XVII. Finally, the normal incidence X-ray imaging system was successful in recording two solar images in the Si XII lines at 44 A. These images are also faint, but show the active region quite clearly. The significant result is that this new technology works and can be used with confidence in future experiments, both in solar physics and in X-ray astronomy.

We encountered several anomalies during the countdown and flight which, while potentially serious, did not affect the mission success. The first of these was a spurious operation of the film transport in the X-ray spectrograph during the T-3 hour check. This coincided with the power-up of SPARCS at about T-240 sec. No command was either transmitted or received by the payload at this time. Normally, SPARCS would already have been under power at this point in the count, and this turn-on was, as we understand it, the result of correction of an earlier operator error. The film transport functioned normally, but was not noticed by the experiment team, since it was unexpected.

At T-130 sec during the same test, we deliberately transmitted the command to advance the X-ray film transport, in order to put a fresh piece of film in place for the flight. This time, the transport mechanism malfunctioned in that the film pressure platen failed to fully retract, and then failed to clamp the film following film advance. This left the system in an anomalous condition, since the system was designed to be launched with the platen clamped. We attempted to clear the anomaly during a second run of the T-3 hour check by re-transmitting the film advance command. Two film advance attempts were unsuccessful. After consulting with my launch team and with the concurrence of D. Paterson, we decided to proceed with the launch anyway, since the X-ray spectrograph was not the prime experiment for this mission. The anomaly cleared itself at T+70 seconds, when the next scheduled film advance command was sent. The transport functioned normally for the remainder of the mission, and the spectrograph produced the required data. As a result of this experience, we now understand the behavior of the film transport both in this flight, and in the flight of 27.054 where the film failed to advance between exposures during the flight. A simple mechanical modification will permanently clear the problem, and will be made and tested prior to the next flight of the system.

Transmission of the command to start the exposure sequence for the soft X-ray imaging system was not successful in the first attempt. This was apparently due to an attempt to send commands too closely spaced in time. The error was discovered at about T+330 sec, and the command successfully re-transmitted. The X-ray imaging system functioned normally thereafter, but only three

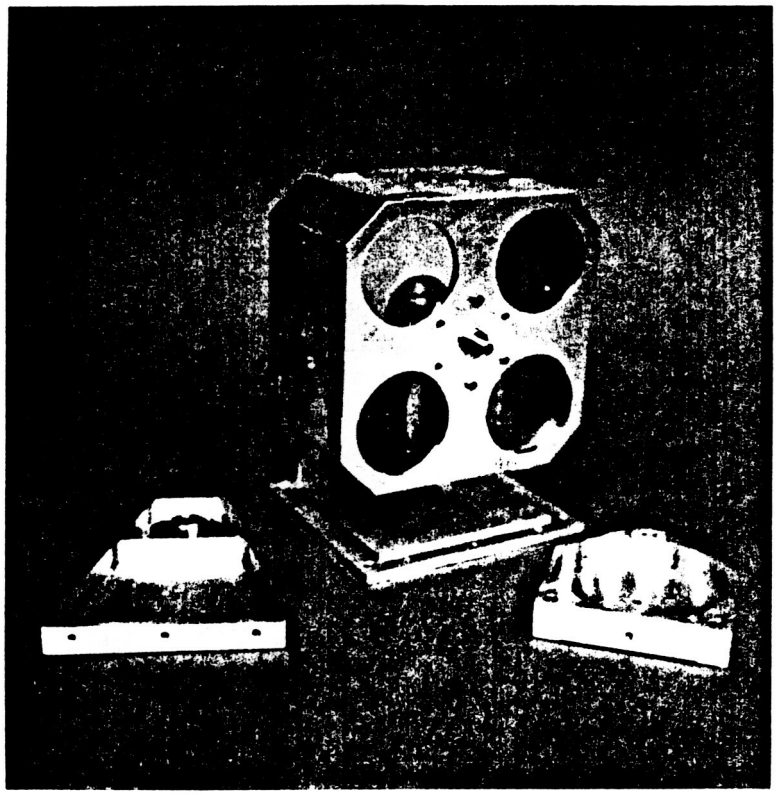

FIGURE 4

frames of the eight frame sequence were exposed. The thin film plastic filter on the front of the first film holder failed, resulting in the loss of one of the frames. The two remaining frames contain solar images.

3.3 Science and Data Analysis Activities

Flight Summary of the XSST/TRC Payload

Rocket (Date)	Configuration		Results
27.032 (3-Jul-79)	XSST:	-Photographic plate, single exposure 10-50A -12 fixed photo-electric channels -UV broadband	-Verified stability of XSST through flight. -Measured alignment of XSST paraboloid from limb crossings. -Good data from UV central image detector.
	TRC:	-Filters 1216A Ly alpha C IV (1550A) C III (977A)	-Excellent Ly alpha images. -Marginal C IV results caused by poor filter quality. -C III filter (thin In film) failed.
27.036 (23-Sep-80)	XSST:	-Same Configuration as 27.032	-Verified alignment and alignment stability. -Marginal results from photoelectric channels. -Good data from central image detector.
	TRC:	-Filters used Ly alpha (1216A) UV continuum	-Excellent images from all channels. Data simultaneous with SMM observations. (1600A)
27.054 (13Jul82)	XSST new film camera new CID		Excellent 10-95A spectrum flare
	TRC (same)		Excellent (50 images)
27.090 (25-Oct-85)	XSST (same)		Good spectrum(>40lines) from active region
	TRC (same)		Excellent (50 images in Ly alpha & 1600A continuum

X-ray Imager	44A lines Image sun using multilayer mirror in normal incidence

- All flights used the H-Alpha via the video link for in flight positioning and post flight data analysis.

3.3.1 Results from 27.Ø36

We were fortunate to be able to conduct the second flight of this payload while the SMM was fully operational. Because of splendid cooperation on the part of everyone involved a data set of unprecedented scope was acquired for NOAA active region 2684. The sub-arcsecond quality TRC images in Lyman alpha and the 16ØØA continuum, formed primarily in the region of temperature minimum, provide complementary data on AR 2684 which is unavailable on any other active regions studied by SMM.

Data from this flight have been analyzed together with observations from SMM and from the vector magnetograph at the MSFC Solar Observatory in a comparison of electric currents computed from the magnetograms with fine structure in the ultraviolet and X-ray ranges. The results are discussed in a paper by Haisch, et al. (1986). An abstract of the paper is included in the appendix.

3.3.2 Results from 27.Ø54

The first two flights of the X-ray spectrograph were troubled by equipment problems unrelated to the spectrograph itself which nevertheless caused the spectrograph data to be lost. These problems were identified and circumvented through re-design of the hardware. On the third flight, our efforts were well rewarded when a magnitude C-8 flare occurred just five minutes before the scheduled launch. We immediately reprogrammed the target region, launched during the rising phase of the flare, and successfully recorded a rich flare spectrum at the time of soft X-ray maximum. The resulting spectrum contained over 4ØØ lines.

Observed wavelengths range from 12.13 A (Fe XVII/Ne IX) to 93.94 A which we attributed to Fe XVIII. The observed range of ionization equilibrium temperatures extends from 7 x 1Ø^5 K, where the Ne VIII lines are formed, to 7 X 1Ø^6, represented by the Fe XIX lines. Emission functions for a number of these lines are shown in Figure 1. Observed ions include C V, C VI, O VII, O VIII, N VI, N VII, Ne VIII, Ne IX, Mg VII-X, Si X-XIII, S XIII, A XIV, Ca XIII-XV and Fe XIII-XIX. The quality of this spectrum, and the wealth of information inherent in it led us to carry out an extended spectroscopic analysis. The results are presented in a paper (Acton et al. 1985, Ap J.)

The spectrum has also been analyzed from the point of view

of the physical conditions in the flaring plasma. In this investigation, we used observed line intensities for ions formed over a range of temperatures to compute the differential distribution of emission measure. Moreover there are several density sensitive transitions in the spectra of helium-like ions enabling us to compute the electron density over the temperature range 0.7 x 10^6 to 3.? x 10^6 K. The density distribution was then used to invert the differential emission measure distribution, resulting in distributions of emitting volume and pressure as a function of temperature. The method also yielded a value for the minimum magnetic field required to confine the plasma. Density diagnostic results are summarized in Brown, et. al., Ap. J. 1986.

3.3.3 Results from 27.090

The object of this flight was to make a coordinated study of small scale structure in weak magnetic fields, Ca II and the ultraviolet continuum. We had enlisted the aid of scientists at several major ground based observatories including Sacramento Peak, the Big Bear Solar Observatory, Kitt Peak Observatory, and zthe MSFC Solar Observatory. The scientific rationale of the study is discussed in detail in our observing proposal to the Sacramento Peak Observatory, included as an appendix to this report.

The primary experiment on the October 25, 1985 flight was the UV imaging with the TRC. Despite questionable Kodak 101.04 high resolution film which was available for the flight, over fifty solar images were recorded. Microdensitometry of the Ca images and magnetograms taken at the Sacramento Peak Observatory during the flight was completed by M. Bruner in August, 1986. A preliminary comparison of the UV cell bright point distribution and the Ca II k2v images was made by Bruner and Dame at LPSP in October, 1986. The predicted correlation appears to have been confirmed, and a more detailed analysis has been planned. A meeting with Dr B. Foing of LPSP was held in Palo Alto in February 1987 to define areas of collaboration on the papers arising from this data set with himself and with Dr. Luc Dame, who served as the scientific leader of the French team for this flight.

A major success of this flight was the first use of multilayer mirror technology for astronomical observations. The unique solar x-ray image in the 44 A spectral interval taken with the normal incidence imager inspired considerable study, resulting in a preliminary paper submitted to Nature, and re-submitted to Science. This paper highlights the unique nature of this technique. A preprint of the paper is included as an appendix to this report.

A spectrum containing over 40 lines in the 20 to 100 A interval was obtained from the XSST. A microdensitometer scan of this spectrum was followed by a preliminary calculation of line intensities and preparation of an emission measure analysis of the emitting plasma. A paper comparing this spectrum, and the

1982 spectrum, with the predictions of Mewe et. al. is in preparation.

We are also combining observations of the XSST, the normal incidence imager, the Flat Crystal Spectrometer of the XRP on SMM, and the ground based magnetometer studies of Kitt Peak and Big Bear solar observatories in a comprehensive analysis of the post flare plasma found in the active region. Collaborators on this analysis include G. Poletto and G. Noci of the Arcetri Astrophysical Observatory in addition to members of the cooperating U.S. observatories.

As in earlier flights, the continuous data stream from the UV central image detector in the XSST was used to verify in flight the coalignment of the instruments. This is done by comparing the video images from the onboard H-Alpha camera with the UV signal as the sun's limb sweeps across the field of view. At least five such crossings ocurred early in the flight and one at the end showed that the pre-flight alignment of the XSST and H-Alpha camera was preserved.

3.3.4 Bibliography

The following is a list of publications and presentations that have been prepared during the performance of this contract.

Published Papers

X-ray Photographs of a Solar Active Region Using a Multilayer Telescope at Normal Incidence, J.H. Underwood, M.E. Bruner, B.M. Haisch, W.A. Brown and L.W. Acton, Science, submitted (1987).

Nonpotential Features Observed in the Magnetic Field of an Active Region, G.A. Gary, R.L. Moore, M.J. Hagyard and B.M. Haisch, Ap. J., **314**, 782 (1987).

Dynamical Behaviour in Coronal Loops, B.M. Haisch, Adv. Space Res., **6**, 45 (1986)

A Comparison of Photospheric Electric Current and Ultraviolet and X-ray Emission in a Solar Active Region, B.M. Haisch, M.E. Bruner, M.J. Hagyard and R.M. Bonnet, Ap. J., **300**, 428 (1986).

New High Resolution Rocket-ultraviolet Filtergrams of the Solar Disc, B. Foing, R.M. Bonnet asnd M. Bruner, Astr. Ap., **162**, 292 (1986).

Electron Density Diagnostics in the 10-100 A Interval for a Solar Flare, W.A. Brown, M.E. Bruner, L.W. Acton and H.E. Mason, Ap. J., **301**, 981 (1986).

Rocket Spectrogram of a Solar Flare in the 10-100 A Region, L.W. Acton, M.E. Bruner, W.A. Brown, B.C. Fawcett, W. Schweizer and R.J. Speer, Ap. J., **291**, 865 (1985).

Characteristic Structures of the Solar Disc Observed on Rocket UV Filtergrams B. Foing and R.M. Bonnet, Astr. Ap., **136**, 133 (1984).

On the Origin of the Discrete Character of the Solar Disk Brightness in the 160 Nanometer Continuum, B. Foing and R.M. Bonnet, Ap. J., **279**, 848 (1984)

Transport and Containment of Plasma, Particles and Energy Within Flares, L.W. Acton, W.A. Brown, M.E.C. Bruner, B.M. Haisch and K.T. Strong, Solar Phys., **86**, 79 (1983).

Rocket Photographs of Fine Structure and Wave Patterns in the Solar Temperature Minimum, R.M. Bonnet, M. Bruner, L.W. Acton, W.A. Brown, M. Decaudin, B. Foing, Astr. Ap., **111**, 125 (1982).

Density and Temperature Determination of Neutral Hydrogen in Coronal Structures, R.M. Bonnet and G. Tsiropoula, Solar Phys., **75**, 139 (1982).

High Resolution Lyman-alpha Filtergrams of the Sun, R.M. Bonnet, E.C. Bruner, L.W. Acton, W.A. Brown and M. Decaudin, Ap. J. Letters, **237**, L47 (1980)

IUE Spectra of G0V-G5V Solar-Type Stars, B.M. Haisch and G.S. Basri, Ap.J. Suppl., **58**, 179 (1985).

NEW ULTRAVIOLET FILTERGRAMS AND RESULTS FROM THE TRANSITION REGION CAMERA EXPERIMENT, L. Dame, B.H. Foing, M. Martic, M. Bruner, W. Brown, M. Decaudin, and R. M. Bonnet (submitted 1986 to Astron & Astrophys)

Presentations

X-RAY, ULTRAVIOLET, OPTICAL AND MAGNETIC STRUCTURE IN AND NEAR AN ACTIVE REGION, B.M. Haisch, T.D. Tarbell, M.E. Bruner, L.W. Acton, R.M. Bonnet and M.J. Hagyard, 165th AAS Meeting, Tucson, Arizona, BAAS, **16**, 1002, (1985).

AN X-RAY EMPIRICAL MODEL OF A SOLAR FLARE LOOP, Marilyn Bruner, William A. Brown, Loren W. Acton, Keith T. Strong, AAS Solar Physics Division Meeting, Bull. Am Astron. Soc. **15**, 1983.

PERFORMANCE OF A SOLAR SOFT X-RAY SPECTROGRAPH-TELESCOPE, W. A. Brown, M. E. Bruner, L. W. Acton, Ann. Israel Phys. Soc. **6**, 1983, p. 60.

12-95 ANGSTROM X-RAY SPECTRUM OF A SOLAR FLARE, Marilyn Bruner, L. W. Acton, and W. A. Brown, 161st AAS Meeting, Boston, Massachusetts, Bull. Am. Astron Soc. 14, 1983.

OBSERVATIONS OF FLARE DENSITY USING HELIUM-LIKE ION LINES. W. A. Brown, M. E. Bruner, and L. W. Acton, Bull. Am. Astron Soc. 14, 898, (1982).

NON-POTENTIAL FEATURES OBSERVED IN THE MAGNETIC FIELD OF AN ACTIVE REGION, G.A. Gary, R.L. Moore, M.J. Hagyard and B.M. Haisch, 168th AAS Meeting, Ames, Iowa, BAAS, 18, 709, (1986).

FLARES: THE SOLAR-STELLAR PERSPECTIVE AND OPPORTUNITIES, B.M. Haisch, presented at Rutherford Appleton Laboratory Workshop: "Flares: Solar and Stellar"; Abingdon, England, May 19-21, (1986).

DYNAMICAL BEHAVIOUR IN CORONAL LOOPS, B.M. Haisch, presented at XXVI COSPAR Meeting, Toulouse, France, June 30 - July 7, (1986).

VARIABILITY IN ACTIVE REGION CORONAL LOOPS, B.M. Haisch, 169th AAS Meeting, Pasadena, California, BAAS, 18, 901, (1986).

FLARE ELECTRON DENSITIES USING X-RAY LINE RATIOS, W.A. Brown, M.E.Bruner, L.W.Acton and H.E.Mason, Solar Physics Division Meeting, Tucson May 1985 (Bull AAS, 17, 1985)

4.0 Appendices

4.1 Abstracts of papers and presentations resulting from the investigation.

4.2 Preprint of a paper discussing emission measure analysis methods, based on the 1982 flare spectrum.

4.3 Proposal to the National Optical Astronomy Observatories for a collaborative investigation supporting the 1985 flight.

4.4 SPARTAN Experimenter's Preliminary Data Package.

4.5 Rocket / SPARTAN Preliminary Design Concept. (following the Challenger accident)

APPENDIX 2

Draft of
The Emission Measure Analysis
Of XSST Data

DRAFT

THE EMISSION MEASURE ANALYSIS OF XSST DATA

M. E. Bruner[1], W. A. Brown[1], A. Fludra[2], J. R. Lemen[3],
H. E. Mason[4], and R. W. P. McWhirter[5]

[1] Lockheed Palo Alto Research Laboratory, Dept 91-20, Building 255, 3251 Hanover Street, Palo Alto, CA 94304, U.S.A.

[2] Astronomical Institute, Wroclaw University, 51-622 Wroclaw, ul. Kopernika 11, Poland

[3] Mullard Space Science Laboratory, Holmbury St Mary, Dorking, Surrey RH5 6NT, U.K.

[4] Department of Applied Mathematics and Theoretical Physics, Silver St.. Cambridge CB3 9EW, U.K.

[5] Astrophysics and Geophysics Div., Rutherford Appleton Laboratory, Chilton, Didcot, Oxon. OX11 0QX, U.K.

Version: 5 June 1987

(Printed on 23 June 1987)

I. INTRODUCTION

Much of our knowledge about the outer layers of the solar atmosphere is based on the interpretation of its spectrum, especially in the vacuum ultra-violet as observed from spacecraft. Thus estimates of plasma velocity (both random and directed) have been made from the profile shapes of spectral lines through the Doppler effect. Line intensity ratios have yielded electron density and temperature estimates while absolute intensities give abundances and information about the structure of the atmosphere through the emission measure method of analysis. In the present paper we examine critically the ability of the emission measure method to provide reliable information about the solar atmosphere. In particular, we use observational data obtained in a recent rocket flight and covering the spectra range 10 Å $\leq \lambda \leq$ 100 Å to build an emission measure model. In our analysis we pay attention to the uncertainties introduced because of errors in atomic data and in the observed intensities as well as the inherent uncertainties of the method itself.

The intensity of a spectral line from an optically thin plasma may be expressed thus:

$$I(p,q) = \frac{1}{4\pi} \int n(p)\, A(p,q)\, dx \qquad \text{photons s}^{-1}\,\text{cm}^{-2}\,\text{sterad}^{-1}, \tag{1}$$

where p and q identify the quantum numbers of the upper and lower levels, respectively, $n(p)$ is the population density (cm^{-3}) of the upper level, and $A(p,q)$ is the spontaneous radiation transition probability (s^{-1}). We assume that the latter can be calculated with some measurable accuracy so that the problem is to find an expression for the population density $n(p)$. The integral is taken over the depth of plasma viewed by the spectrometer. This will depend on where the spectrometer is pointed and on its field of view. If, as for the present spectrometer, the field of view is small and it is pointing at the solar disk, then the integral is taken as summing from the chromosphere to the top of the corona. In other cases where the spectrometer is pointed above the limb or views the whole disk, other considerations determine the range of the integral.

In a low density plasma of the kind we are concerned with the population density $n(p)$ of an excited level is determined by many collisional and radiation processes. However, generally only one or two of these are dominant with the others providing a negligible effect. Thus it is often adequate to write

$$n(p) = n_e n(z,g)\, X'(g,p) / \sum_r A(p,r)\,, \tag{2}$$

where n_e is the electron density, $n(z,g)$ the population density of ions of the relevant charge z in the ground level, $X'(g,p)$ is the collisional excitation rate coefficient, and $\sum_r A(p,r)$ the sum of the radiative decay probabilities out of level p. We discuss later the applicability of this simple expression to cover a multitude of processes but note here that $X'(g,p)$ is an effective coefficient that goes some way to taking account of the secondary processes.

Equations (1) and (2) may now be combined so that with some re-arrangement become

$$I(p,q) = \frac{1}{4\pi}\frac{n(Z)}{n(H)}\int \frac{n(z,g)}{n(Z)}\,X'(g,p)\,\frac{n(H)}{n_e}\,n_e^2\,dx\,\frac{A(p,q)}{\sum_r A(p,r)}\,, \tag{3}$$

where $n(Z)$ and $n(H)$ are the population densities of the relevant element and of hydrogen (neutrals + ions). At this point we have made the important assumption that the element abundance is constant throughout the depth of the atmosphere. We note that the terms inside the integral may be grouped into two factors with one dependent only on atomic physics and usually given the symbol $G(p,q,T_e)$ where

$$G(p,q,T_e) = \frac{n(z,g)}{n(Z)}\,X'(g,p)\frac{n(H)}{n_e}\,\frac{A(p,q)}{\sum_r A(p,r)}\,, \tag{4}$$

and the other describing the structure of the solar atmosphere. This latter factor contains the kernel of the quantity known as the emission measure. At this stage various authors have chosen different ways of proceeding. Here we confine ourselves to models of the atmosphere where the electron temperature (T_e) depends monotonically on position so that we may write

$$I_j = \frac{1}{4\pi}\frac{n(Z)}{n(H)}\int_{T_1}^{T_2} G_j(T_e)\,n_e^2\,\frac{dx}{dT_e}\,dT_e\,, \tag{5}$$

and define

$$\varphi(T_e) = n_e^2\,\frac{dx}{dT_e} \qquad \mathrm{cm}^{-5}\,\mathrm{K}^{-1} \tag{6}$$

as the differential emission measure. Note that in equation (5) and in the subsequent discussions we denote the spectral line by the index j, instead of the quantum numbers p and q. The range of the integral now runs from a temperature characteristic of the chromosphere ($< 10^4$ K) to one characteristic of the top of the corona ($> 2 \times 10^6$ K). We return to this choice below.

It is important to recognize the form of the $G_j(T_e)$ function. Expressing it in this way implies that it is a function only of T_e, which it is. But in some cases $G_j(T_e)$ is also a function of n_e — for the so-called density sensitive lines. Moreover, implicit in the dependences are the assumptions that (a) the plasma is in steady-state ionization balance and (b) the electron distribution is Maxwellian. If either of these assumptions breaks down the analysis becomes much more complex. In what follows we assume Maxwellian electron velocity distributions and steady-state ionization balance. For the moment we will neglect the density dependence but will return to this point below. In any case, the dependence on temperature is much stronger than on density. The ionization balance ratio has a dominant effect and ensures that $G_j(T_e)$ is negligible except over a limited range of temperature in the neighbourhood of T_M, the temperature at which it has its maximum value. Some authors find it useful to introduce somewhat

arbitrarily the integral of the square of the electron density over a distance defined between the positions in the model atmosphere where the electron temperature has the values $T_M/\sqrt{2}$ to $\sqrt{2}\,T_M$ which yields a quantity called the emission measure, EM defined as

$$EM = \int_{T_M/\sqrt{2}}^{\sqrt{2}T_M} \varphi(T_e)\, dT_e \qquad \mathrm{cm}^{-5}. \tag{7}$$

Despite its arbitrariness it has the virtue of drawing attention to the fact that the shape of the $G_j(T_e)$ function determines the fundamental temperature resolution of the method. It is clear that there are an infinite number of possible functions $\varphi(T_e)$ that satisfy the equations (5) and (6). However, those with sharper variations with T_e than that consistent with the shape of the relevant $G_j(T_e)$ functions are clearly not justified on the basis of the data.

We now consider some of the finer points of the atomic physics as it pertains the analysis described above. We start with line pairs from the same ion whose intensity ratio is a function of temperature but is virtually independent of density — for example Li-like 2–2 to 2–3 transitions. Such lines sample different regions of the atmosphere and may thus be used to determine the ratio of the emission measures of these regions without the uncertainties associated with abundances usually present. In this connection it is worth examining the contribution functions $G_j(T_e)\varphi(T_e)$ of the intensity integrals given in equation (5). It should be emphasized here that the use of line ratios regarded as temperature sensitive in analyses of this kind is not a particularly helpful way of estimating the electron temperature, but does lead to a useful method of determining the shape of the emission measure distribution.

Line pairs whose intensity ratio is density sensitive can also be given special treatment. In this case we introduce another assumption, viz. that since the lines are emitted from a relatively narrow region in the solar atmosphere, it is reasonable to assume that the plasma pressure over that region is constant. Thus we introduce a quantity $p(T_M) = n_e T_e$ = constant in the region about T_M. Equation (5) may be written as follows:

$$I_j = \frac{1}{4\pi}\frac{n(Z)}{n(H)} \int_{T_1}^{T_2} G_j(T_e, n_e)\varphi(T_e)\, dT_e\,, \tag{8}$$

where $G_j(T_e, n_e)$ is written thus in recognition of its dependence on both T_e and n_e. This $G_j(T_e, n_e)$ function may be evaluated for a set of values of $p(T_M) = n_e T_e$ and the integral evaluated for both lines using the best available estimates of $\varphi(T_e)$ over the relevant range. Thus the calculated intensity ratio may be determined as a function of $p(T_M)$ and compared with the observed ratio to determine $p(T_M)$ relevant to that temperature range. Since this method also depends on taking ratios of intensities for the same ion the result is independent of the abundance value. In addition it is to some extent independent of the ionization balance calculation, especially where the excitation functions have similar dependencies on temperature. Note however, that the value of T_M is dependent on the ionization balance calculation.

II. DESCRIPTION OF THE SPECTRAL DATA

A grazing incidence X-ray spectrograph covering the wavelength region 10–95 Å was flown on board a sounding rocket on 1982 July 13. The instrument was pointed at the soft X-ray emission from a flare which peaked in intensity at 1627 UT, 2 minutes prior to the observations. Two exposures were obtained: the first lasting 54s and the second 145s. Unfortunately, the film transport mechanism failed and the film only advanced 0.5 mm. This is, however, sufficient to separate the two spectra. The spectra are rich in lines covering the temperature range 5×10^5 K – 5×10^6 K. A detailed discussion of the experiment and a complete list of identifications is given in Acton *et al.* (1985). A study of electron density diagnostics for these spectra is given in Brown *et al.* (1986). The electron density was found to be constant at about 3×10^{10} cm^{-3} over the entire temperature range for this flare. A brief discussion of the flare morphology and a preliminary differential emission measure analysis was presented by Acton *et al.* (1983). In this paper we present a detailed study of different techniques for obtaining the differential emission measure.

III. ASSESSMENT OF OBSERVED ERRORS

Spectral line intensities are given in table 3 of Acton *et al.* (1985). We have re-assessed the systematic and random errors in those values. The intensity is defined in equation (1) of Acton *et al.* (1985) as:

$$I_\lambda = U_\lambda \, dw \quad \text{photons cm}^{-2}\,\text{s}^{-1}\,\text{arcsec}^{-2}, \tag{9}$$

where where d, the peak density and w, the FWHM, are related to the height and FWHM in mm of the spectral lines on the densitometer scans. Measurements were made with a magnifying glass incorporating a scale and the errors are typically 6 per cent. The values of U_λ are given by equation (2) of Acton *et al.* (1985) as:

$$U_\lambda = \frac{0.0024 L_\lambda (E/d)_\lambda}{A T \Omega E m_\lambda E g_\lambda}, \tag{10}$$

where L_λ is the line length from full mirror width, $(E/d)_\lambda$ = exposure density for the film, A is the effective mirror area for the full mirror width, T is the exposure time (145s) and Ω=33 arcsec^2 (the nominal field of view), Em_λ is the efficiency of the paraboloidal telescope mirror, Eg_λ is the efficiency of the concave spectrograph grating. The parameters $(E/d)_\lambda$, Em_λ, and Eg_λ are given in table 1 of Acton *et al.* (1985) and were measured pre- and post-flight. Of the five wavelengths at which grating efficiency was measured, the largest discrepancy before and after the flight was in Eg at 8.34Å. This was measured as 0.01 before and 0.05 after the flight. The post flight value was used in preference. The values $(E/d)_\lambda$ represent the response of the photographic plate. The type of plates used have been studied in detail, both theoretically and experimentally, by Henke *et al.* (1984), who found a constant response. Based on

Henke *et al.*'s results the values of $(E/d)_\lambda$ given in table 1 of Acton *et al.* (1985) should probably be constant, and therefore, we have adopted $(E/d)_\lambda = 3 \times 10^8$ and have re-calculated $\log_{10} U_\lambda$ as a function of $1/\lambda$ accordingly. The fit of $\log_{10} U_\lambda = 5.7916/\lambda + 3.133$ (equation (3) of Acton *et al.*) was used by Acton *et al.* to obtain intensities. We use the curve given in Figure 1, which fits our re-scaled $\log_{10} U_\lambda$ values. The random errors in *Em* are 8 per cent and *Eg* are 15 per cent giving a combined error of 17 per cent.

We considered the effect of atmospheric absorption within the instrument which is largest for the long wavelength lines. However, this was found to be negligible since the second exposure, during the rocket descent, which finished above 160 km. The rocket was evacuated before launch and the vacuum door was re-opened in flight to re-evacuate the instrument. A small pressure builds up inside the film holder as the result of evaporation from the container and film. This could have reduced the intensities for the longer wavelength lines which were at the end of the photographic plate furthest from the vacuum, by up to 10 per cent.

IV. SPECTRAL LINE INTENSITIES

In table I we list the lines which have been selected for the differential emission study. These lines were chosen to cover as wide a temperature range as possible. They are first order lines from the second, longer exposure. They were chosen to be relatively free from blending with higher order lines and first exposure lines. In table II we list line intensities and error estimates. In the previous section we discussed systematic and random errors. Errors for individual lines depend on their strength and the proximity of blends.

[Describe the atomic data here? Abundances?]

V. DIFFERENTIAL EMISSION MEASURE ANALYSIS

The presence of several lines in the *XSST* flare spectra which are are formed over a range of temperatures indicates that the emitting plasma is far from isothermal. In the past, several authors (e.g., Withbroe, 1975; Parkinson, 1975; Sylwester, Schrijver, and Mewe, 1980; Fludra and Sylwester, 1986) have suggested techniques for the multi-thermal analyses of solar spectra with various degrees of sophistication. The objective of such analyses is to determine the differential emission measure, $\varphi(T_e)$ (see equation [6]). To do this it is necessary to deconvolve $\varphi(T_e)$ from the measured spectral intensities, given the $G_j(T_e)$ functions for the individual lines. This is typically accomplished by assuming an initial form for the differential emission measure, $\varphi_0(T_e)$ from which theoretical line intensities are calculated and subsequently compared with the observed line intensities. Based on this comparison, a new differential emission measure, $\varphi_1(T_e)$ is postulated and further iterations are performed until convergence is achieved. In practice this may be cumbersome, yet the problem is well suited to computer analysis

techniques. There are several techniques which can be used for this purpose. Since there are many solutions for $\varphi(T_e)$ which satisfy the set of equations (5) and (6) to within the uncertainties, the main difficulty is to choose the best solution. Following the approach taken by Fludra and Sylwester (1986), solutions obtained with different techniques will be considered for the *XSST* flare spectrum.

By way of illustration we make, for a moment, a simplfying assumption: the $G_j(T_e)$ functions are replaced by a value averaged over the temperature range where it has its peak value. This is justifiable since $G_j(T_e)$ is generally peaked at some temperature T_M. In this case the line intensities may be expressed as:

$$I_j = \frac{1}{4\pi}\frac{n(Z)}{n(H)}\langle G(T_M)\rangle_1 \int_{T_M/\sqrt{2}}^{\sqrt{2}T_M} \varphi(T_e)\, dT_e, \tag{11}$$

where we have taken the same temperature limits for the integral of $\varphi(T_e)$ as was assumed for equation (7). Combining equations (5), (6), and (11) we obtain

$$\langle G_j(T_M)\rangle_1 = \frac{\int_{T_1}^{T_2} G_j(T_e)\varphi(T_e)\, dT_e}{\int_{T_M/\sqrt{2}}^{\sqrt{2}T_M} \varphi(T_e)\, dT_e}. \tag{12}$$

By defining the averaged value of the $G_j(T_e)$ function for any particular line j in this rather formal way it is possible to devise a practical and fully consistent analysis procedure. Thus, an arbitrary but approximately correct value of the $G_j(T_e)$ functions is to take, for example, 2/3 of its maximum value:

$$\langle G_j(T_M)\rangle_0 = \frac{2}{3}[G_j(T_e)]_{\text{Peak}}, \tag{13}$$

which is used to calculate a first estimate of the emission measure at T_M as:

$$EM_0(T_M) = \frac{4\pi I_j n(H)}{\langle G_j(T_M)\rangle_0\, n(Z)}. \tag{14}$$

This is related to the average value of the differential emission measure at T_M as:

$$EM_0(T_M) = \varphi_0(T_M)\int_{T_M/\sqrt{2}}^{\sqrt{2}T_M} dT_e = \varphi_0(T_M)\, T_M/\sqrt{2}, \tag{15}$$

so that the value of $\varphi(T_M)$ can be found at all the temperatures T_M for which spectral line intensities are available. A curve may now be drawn through these points to give a first approximation of the differential emission function, $\varphi_1(T_e)$. This may then be used in equation (12) to derive a better average value of the $\langle G_j(T_M)\rangle$ function and the process is repeated by using $\langle G_j(T_M)\rangle_1$ in place of $\langle G_j(T_M)\rangle_0$ in equation (15). Iteration to a converged solution may then be possible.

In the preceeding discussion we made the simplifying assumption that $G_j(T_e)$ is replaced by a temperature-averaged function $\langle G_j(T_M)\rangle$ which is removed from the temperature integral. This illustrates the nature of the iterative procedure to obtain $\varphi(T_e)$. In the next sections we discard this assumption and return to the problem of solving equations (5) and (6). Three numerical procedures are presented and tested on *XSST* flare spectra.

It is necessary to evaluate the integral given in equation (5) in order to compute the calculated intensities, I_j. The integration is done numerically by summing the integrand over a large number of small-temperature intervals of equal size in $\ln T_e$. If the integration is performed logarithmically over T_e equations (5) becomes

$$I_j = \frac{1}{4\pi}\frac{n(Z)}{n(H)}\int_{\ln T_1}^{\ln T_2} G_j(T_e)\varphi(T_e)\, T_e\, d(\ln T_e)\,, \tag{16}$$

and the expression for $\varphi(T_e)$ (equation [6]) becomes

$$\varphi(T_e) = n_e^2\,\frac{dx}{d(\ln T_e)}\,. \tag{17}$$

In the analysis here and in the subsequent sections we have taken $d(\ln T_e) = 0.115$ as the step size for the numerical integration.

The value of χ^2 is computed to evaluate the solution of $\varphi(T_e)$, where χ^2 is given by:

$$\chi^2 = \sum_{j=1}^{N}\frac{(O_j - I_j)^2}{\sigma_j}\,, \tag{18}$$

and O_j are the measured intensities, I_j are the intensities computed using equations (16) and (17), and σ_j are the uncertainties of O_j. The summation over j refers to the number of lines, N, included in the analysis.

The three numerical techniques considered below satisfy the general condition that $\varphi(T_e) \geq 0$. Craig and Brown (1976a,b) have criticised the multithermal analyses of X-ray spectra based on a mathematical model which did not meet this criterion. It is clear that only techniques which exclude *a priori* negative values of emission measure should be used in this type of analysis.

a) Withbroe-Sylwester technique

The first technique which we investigate was suggested by Sylwester, Schrijver, and Mewe (1980) who based their work on a weighting factor method given Withbroe (1975) and in the subsequent discussion we will refer to this method as the Withbroe-Sylwester technique. This technique computes the next approximation of the the differential

emission measure distribution, $\varphi_{i+1}(T_e)$, based on the value of $\varphi_i(T_e)$ by means of the expression:

$$\varphi_{i+1}(T_e) = \varphi_i(T_e) \frac{\sum_{j=1}^{N} W_j(T_e) R_j}{\sum_{j=1}^{N} W_j(T_e)}, \tag{19}$$

where, $R_j = (O_j/I_j)$; O_j and I_j are the observed and computed line intensities, $W_j(T_e)$ is an empirical weighting function, and the summation over j corresponds to the N different lines included in the analysis. The weighting function of Withbroe (1975) was modified by Sylwester, Schrijver, and Mewe (1980) to take into account uncertainties in the measurements of the line intensities and was defined as

$$W_j(T_e) = G_i(T_e)\varphi_i(T_e) \frac{\int_0^\infty G_j(T_e)\varphi_i(T_e)\, dT_e}{\int_0^\infty [G_j(T_e)\varphi_i(T_e)]^2 dT_e} [D_j + 1]^a , \tag{20}$$

where $D_j = (|O_j - I_j|/\sigma_j)$; σ_j is the uncertainty of the observed intensity O_j, and $a \geq 0$ if $O_j \geq I_j$, else it is negative.

Figure 2a shows the differential emission measure, $\varphi(T_e)$, obtained for the *XSST* flare spectrum using the Withbroe-Sylwester technique. A description of the spectral line intensities and the atomic data and solar abundances used to compute the calculated line intensities is given in §IV. In Figure 2b is plotted the observed intensities (O_j) and uncertainties as error bars and the computed intensities (I_j) are shown as circles plotted as a function of the temperature T_M which corresponds to the value at which $G_j(T_e)$ has its maximum. By comparing Figures 2a and 2b it is possible to estimate which lines are responsible for the resulting shape of the differential emission function.

We see from Figure 2b that the technique is successful in predicting the intensities to within the 1σ uncertainties of almost all the observed line intensities. The intensities of three lines are shown as triangles and these lines were excluded from the analysis because agreement between the theoretical and observed intensities could not be achieved. Two of these lines are formed in Fe XVII and Fe XVIII (lines 5 and 27 in table I) and we note that the disagreement between theory and observation is in the opposite sense for the two lines. The source of this disagreement is either because of an error in the instrumental calibration or in the excitation rates or some combination of the two. [Mention C VI disagreement.]

Although the observed intensities have been fit by the differential emission measure distribution shown in Figure 2a, it is observed that the actual shape of $\varphi(T_e)$ has several sharp features. Because the expression in equation (16) for the line intensities is an integral over $G_j(T_e)$ and $\varphi(T_e)$, the line intensity values are relatively insensitive to features in the shape of the $\varphi(T_e)$ curve which are narrower than the $G_j(T_e)$ functions themselves. Given this and the deconvolution nature of this problem, it becomes clear that a family of solutions for $\varphi(T_e)$ will produce the same or similar results for the calculated line intensities. Therefore, the empirical weighting function, $W_j(T_e)$, was

introduced in order to choose a solution of $\varphi(T_e)$ which varies smoothly with temperature, and presumably represents, in a physical sense, the "simplest" of all possible solutions. However, when a discrepancy exists between the data and the theory — for example, when two lines formed at nearly the same temperature have observed intensities which no value of $\varphi(T_e)$ can provide simultaneously — the algorithm may adjust $\varphi(T_e)$ to represent a physically unlikely solution. This probably explains the present of sharp features observed in the differential emission curve (Figure 2a) which correspond to T_M of the various $G_j(T_e)$ functions.

b) Withbroe-Sylwester technique – 1σ approximation

The Withbroe-Sylwester technique attempts to adjust the differential emission measure distribution until the calculated intensities are exactly equal to the observed intensities. When this happens R_j is unity for all values of j and the convergence of equation (19) is completed. As a result, errors in the values of O_j will effect the final solution for $\varphi(T_e)$. We modified this technique to provide solutions for $\varphi(T_e)$ which are less affected by possible errors in the observed intensities and yet still satisfy the requirement of predicting values of the line intensities to within their estimated uncertainties.

The main difference between this and the exact version of the Withbroe-Sylwester technique is that the functions R_j in equation (19) are modified so that a change to $\varphi(T_e)$ occurs only if the predicted intensity differs from the observed intensity by more than 1σ. Thus, we set

$$R_j = \begin{cases} (O_j - \sigma_j)/I_j & \text{if } I_j < O_j - \sigma_j; \\ 1 & \text{if } |O_j - I_j| \le \sigma_j; \\ (O_j + \sigma_j)/I_j & \text{if } I_j > O_j + \sigma_j. \end{cases} \tag{21}$$

A 1σ limit in this definition of R_j is chosen because our σ_j is a maximum uncertainty of O_j. In fact, a family of solutions can be computed, using different values $\alpha\sigma_j$, for α decreasing from, say, 3 to 0. The solution for a given α can be the initial approximation for the next, lower α. For $\alpha = 0$ we obtain again the original Withbroe-Sylwester solution. The upper limit for α should be between 1 and 3, depending on whether σ_j is the maximum error of O_j, or it has a purely statistical meaning. We also modified the expression for D_j to be

$$D_j = \begin{cases} (O_j - I_j)/\sigma_j - 1 & \text{if } I_j < O_j - \sigma_j; \\ 0 & \text{if } |O_j - I_j| \le \sigma_j; \\ (O_j - I_j)/\sigma_j + 1 & \text{if } I_j > O_j + \sigma_j. \end{cases} \tag{22}$$

Although the modification specified in equation (22) can influence the convergence of the algorithm, it is not an essential aspect of the 1σ method.

The results of this procedure for $\alpha = 1$ are shown in Figure 3. With this technique the shape of the differential emission curve has less sharp features, but there are still

indications that the observed shape is influenced by the $G_j(T_e)$ functions, and thus the individual features may not be physically meaningful. As expected, this technique resulted in a larger value of χ^2 because the algorithm did not attempt to modify the solution when all the predicted line intensities agreed with the observed intensities to within the $\pm 1\sigma$ uncertainties.

c) Exponential polynomial version As a third approach we assumed the shape of the differential emission measure to be described by the exponential of a polynomial given by

$$\varphi(T_e) = \beta e^{\omega(T_e)}, \tag{23}$$

where β is the normalization constant and $\omega(T_e)$ is a polynomial function of the electron temperature given by:

$$\omega(T_e) = \sum_{k=1}^{M} a_k P_k(T_e), \tag{24}$$

where P_k is a Chebyshev polynomial of order k. Using this technique the coefficients of the polynomial function, $\omega(T_e)$ are varied iteratively to minimize the value of χ^2 given by equation (21) and by choosing the lowest order polynomial which will provide an acceptable fit, it is possible to obtain a solution for $\varphi(T_e)$ whose shape is not governed so explicitly by the form of the $G_j(T_e)$ functions. Although this is a positive aspect of this technique, there is the corresponding disadvantage that the assumed function may not be appropriate to describe the real $\varphi(T_e)$. The use of Chebyshev polynomials ensures that the coefficients, a_k, are all of roughly the same order of magnitude and makes the search for the best solution over parameter space better conditioned.

The result of fitting the *XSST* data with the exponential polynomial technique is shown in Figure 4. The shape of $\varphi(T_e)$ agrees overall with the results from the previous techniques but is smoother. The displayed result was obtained with a fifth order polynomial. We found that polynomials with higher orders gave essentially the same solution with only a small change in the total value of χ^2.

VI. DISCUSSION

VII. CONCLUSION

REFERENCES

Acton, L. W., Brown, W. A., Bruner, M. E. C., Haisch, B. M., and Strong, K. T. 1983, *Solar Phys.*, **86**, 79.

Acton, L. W., Bruner, M. E., Brown, W. A., Fawcett, B. F., Schweizer, W., and Speer, R. J. 1985, *Ap. J.*, **291**, 865.

Brown, W. A., Bruner, M. E., Acton, L. W., and Mason, H. E., 1986 *Ap. J.*, **301**, 981.

Craig, I. J. D. and Brown, J. C. 1976a, *Nature*, **264**, 340.

Craig, I. J. D. and Brown, J. C. 1976b, *Astron. Astrophys.*, **49**, 239.

Fludra, A. and Sylwester, J. 1986, *Solar Phys.*, **105**, 323.

Henke, B. L., Fujiwara, F. G., Tester, M. A., Dittmore, C. H., and Palmer, M. A., 1984, *J. Opt. Soc. Am. B*, **1**, 828.

Parkinson, J. H. 1975, *Solar Phys.*, ,.

Withbroe, 1975, *Solar Phys.*, **45**, 301.

Sylwester, J., Schrijver, J., and Mewe, R. 1980, *Solar Phys.*, **67**, 285.

APPENDIX 3

Scientific Proposal
to the
National Optical Astronomy Observatories
for a
Collaborative Investigation
supporting the
1985 Rocket Flight

A SCIENTIFIC PROPOSAL
for
A COORDINATED STUDY OF SMALL SCALE STRUCTURE
in
WEAK MAGNETIC FIELDS, Ca II AND THE UV CONTINUUM

Principal Investigator

Dr. Marilyn Bruner
Lockheed Palo Alto Research Laboratory
Palo Alto, Ca.

Co Investigators

Dr. William. A. Brown
Lockheed Palo Alto Research Laboratory
Palo Alto, Ca.

Dr. Luc Dame
Laboratoire de Physique Stellaire et Planetaire
Verrieres le Buisson, France

A SCIENTIFIC PROPOSAL
for
A COORDINATED STUDY OF SMALL SCALE STRUCTURE
in
WEAK MAGNETIC FIELDS, Ca II AND THE UV CONTINUUM

Marilyn Bruner
Lockheed Palo Alto Research Laboratory
Principal Investigator

ABSTRACT

This proposal covers an experimental program whose object is to study the relationship between structures that can be seen in spectroheliograms made in the ultraviolet continuum near 1600 A, and structures that are visible in the K2V wing of the Ca II K line. Both types of observations show a pattern of small, compact bright points that are found in the interior of cells in the supergranulation network. These two types of points have similar sizes and spatial frequency distributions, suggesting that they may represent a common phenomenon. Moreover, in high quality magnetograms, one can see a pattern of small magnetic features that also have the same size and spatial frequency characteristics. The purpose of this proposed observational program is to test the hypothesis that all three sets of features are associated, which would strongly imply the existence a physical mechanism connecting them. The experimental approach is to make simultaneous observations of the UV structures from a sounding rocket flown from the White Sands Missile Range, and of the Ca II K2V and the magnetic structures from the Tower instruments at the Sacramento Peak Observatory.

BACKGROUND

Cell Bright Points

The Ca II K2V structures and their temporal behavior have been studied in detail by Liu et al, (1972) and Liu (1972) who give references to earlier work. Of particular interest to us is Liu's discussion of cell points. These are small, isolated bright features located inside the cells of the supergranulation network. They are distinct from the loosely connected strings of bright points that form the network itself, and their temporal behavior is quite different. There are typically 5 to 10 cell points in the interior of a cell. Lifetimes of cell points range from 30 to 100 seconds, with an average of about 50 seconds. Fig 1, reproduced from Liu's thesis, illustrates the light curve of a typical cell point.

Some cell points exhibit an oscillatory behavior, as shown in Fig 2, also reproduced from Liu's work. Note that there is a well defined peak in the power spectrum at a period of about 200 seconds. Liu's studies of the Ca II K line profiles of cell points show that the intensity fluctuations are most pronounced in the K2V wing of the profile, but can be seen throughout the central part of the profile. He takes particular note of his observation that the fluctuations are in phase throughout the line profile, though the amplitude is a maximum at K2V.

Based on Liu's discussion, we may reasonably expect to observe a substantial number of cell points within the field of view of the Universal Birefringent Filter, and to follow their growth and decay cycles during the

five minute observing period available during the rocket flight.

Magnetic Field Structures

A correspondence between the cell bright points seen in the Ca II K2V spectroheliograms and small scale structure in photospheric magnetic fields has been reported by Sivaraman and Livingston (1982). They used the 512 channel magnetograph to alternately observe the 8688 A line of Fe I and the K2V line of Ca II. They took account of the different time behaviors of the K2V features (50 sec lifetimes) and the magnetic field patterns (typically one hour) by interleaving pairs of magnetograms with bursts of K2V images. The time resolution of each burst was less than 10 seconds, in order to assure that the light curves of the cell points were fully resolved.

Their results appear to show that each cell point is spatially correlated with a local maximum in the magnetic field. The polarity of the field did not seem to matter; correspondences with both positive and negative polarity were found. The correspondence was not one-to-one; that is, not all maxima in the weak magnetic field pattern showed cospatial cell bright points, even though the reverse appears to be true. They suggest that the mechanism responsible for producing the cell bright points is guided by the field, which would explain the observation of recurrent points reported by Liu. Sivaraman and Livingston also report a tendency for the strength of the magnetic field to be correlated with the maximum brightness attained by a cell point.

UV Continuum Bright Points

Observations of the UV continuum near 1600 A were made during a series of rocket flights conducted by this laboratory in collaboration with Dr. R. M. Bonnet who, at that time, was the director of the Laboratoire de Physique Stellaire et Planetaire in France. These observations were discussed by Bonnet et al. (1982) who drew attention to the similarity of the distribution of bright UV grains to that of the cell points described by Liu et al. Bonnet et al. also discussed the origin of the 1600 A continuum and pointed out its very high sensitivity to temperature fluctuations in the temperature minimum region. Fig 3, reproduced from their paper, illustrates the UV continuum appearance, and clearly shows the bright grains.

APPROACH

In order to test the hypothesis that the three distributions discussed above are, in fact, cospatial; we propose to conduct simultaneous observations of the UV continuum, the magnetic field distribution, and the Ca II K2V patterns. The UV observations would be made during a sounding rocket flight which is currently scheduled for October 22nd, 1985 at the White Sands Missile Range. The magnetograms and Ca II images would be made from the Tower at the Sacrament Peak Observatory. The selection of the time of day for the rocket launch will be made in consultation with the Sacramento Peak staff so as to optimize the conditions for good seeing. In the event that we are unable to launch at the chosen time or that the seeing is inadequate, we have a backup launch opportunity scheduled for October 25th.

Rocket Observations

The rocket will carry three prime instruments and one auxiliary

instrument. The prime instruments are the ultraviolet filtergraph, a soft X-ray spectrograph and a normal incidence soft X-ray imaging system operating at the 44 A line of Si XII. The UV filtergraph is considered to be the prime experiment for this flight. The fourth instrument is an H-alpha imaging system that transmits a television image back to the ground for use in pointing the payload at the desired region.

The Ultraviolet filtergraph carries four filters, two for H-lyman alpha and two for the 1600 A continuum. The two 1600 A filters have different short wavelength cutoffs, chosen so that the difference between their two images will have enhanced response to the C IV lines at 1548 and 1550 A. These difference images should give us an idea of the distribution of transition zone material in the vicinity of active regions (if any!) and will probably respond to the network. It will be interesting to see whether there is any indication of transition zone material in the vicinity of the cell points, though this is not a major objective of the experiment. The field of view of the filtergraph is somewhat larger than the sun, so that in-flight co-alignment of the fields of view of the rocket and the Sac Peak instruments is not a major concern. The UV filtergraph will make three exposure sequences, each lasting about 80 seconds and including a range of exposures through each of the four filters.

The X-ray imaging system is a normal incidence prime focus telescope, consisting of a simple spherical mirror, a mechanical shutter, and an eight position film cassette. The mirror is coated with a layered synthetic microstructure (LSM), which performs as an artificial bragg crystal whose 2d spacing is equal to the desired X-ray wavelength. It has the property of a relatively high reflectivity (about 10%) at the chosen X-ray wavelength, and a negligible response at nearby wavelengths. Visible and ultraviolet radiation are excluded from the system by thin metal-coated plastic film filters that cover each film holder in the cassette. The line we have selected for this flight is sensitive to plasma in the two million degree range characteristic of the quiet corona.

The X-ray spectrograph is a glancing incidence grating instrument with a parabolic sector mirror that serves as a light collector. It is capable of recording spectra in the 20 to 120 A range, which covers the temperature range 0.5 to 10 million degrees. If there is any solar activity on the day of launch, we will attempt to record the X-ray spectrum of an active region.

After launch, the rocket will require approximately 100 seconds to reach observing altitude and acquire the sun. If there is a suitable active region present, we will conduct a pattern search for the brightest point before beginning our exposures. This is expected to take an additional 70 seconds. The rocket is expected to re-enter the atmosphere about 490 seconds after launch, allowing us a little over 5 minutes of usable observing time for the three UV filtergraph sequences and the eight X-ray images. The X-ray spectrograph will make a single exposure lasting for the entire 5 minute observing period. The rocket is expected to be back on the ground about 15 minutes after launch, and will be recovered for processing of the flight film.

Sacramento Peak Observations

As discussed with Drs. R. Smartt and J. Zirker, we would like to have observations made with the Universal Birefringent Filter of the 6302 A line in the magnetogram mode, and with the Ca K filter of the K2V feature (-0.18 A from line center). These observations should be made during the pre-launch

and early phases of the rocket flight. The repetition rate should be of the order of two seconds in order to resolve the temporal behavior of the cell bright points, and to give us a better chance of catching moments of better seeing. At some point at or near the end of the data taking portion of the rocket flight, we would like to shift to the echelle spectrograph, and observe the Ca II K line profiles over a field of view of the order of 1 x 1 arc minute, and with a repetition rate of the order of 30 seconds. This is the mode developed by Dr. Dame during his last visit to Sac Peak last July and August.

It would also be quite interesting to have H-alpha images emphasizing the solar limb if they can be made without interfering with the primary program. The objective here is to compare the limb observations of H-alpha and lyman alpha to see how the sizes of prominences and spicules compare in the two lines. It has been my impression in studying our previous lyman alpha images that there is a very distinct diffuse component to the lyman alpha structures that is not evident in H-alpha. If we can show that there is a lyman alpha "halo" around the H-alpha features above the limb, we may have evidence for ambipolar diffusion. We may also find structures in lyman alpha that are not evident in H-alpha, as the former is expected to be more easily excited by the resonant scattering process.

The requested observing sequences from the Tower are summarized as follows:

PRE-LAUNCH PHASE:

- UNIVERSAL BIREFRINGENT FILTER MAKES MAGNETOGRAMS AT 6302
  RECORDING MEDIUM: FILM
  REPETITION RATE: 2 SEC (APROX)
  FIELD OF VIEW: 3 X 3 ARC MINUTES
  BEAM STABILIZATION USING SAC PEAK SYSTEM IF A SUNSPOT IS AVAILABLE

- K LINE FILTER IS OPERATED AT K2V WITH BANDPASS OF 0.3 A
  RECORDING MEDIUM: FILM
  REPETITION RATE: 2 SEC (APROX)
  FIELD OF VIEW: 3 X 3 ARC MINUTES
  BRANCH FEED USED TO GET SIMULTANEOUS, COSPATIAL OBSERVATIONS

EARLY FLIGHT PHASE:

Above program continues throughout ascent phase and for the first two UV filtergraph sequences.

LATE FLIGHT PHASE:

This phase lasts from the start of the third UV filtergraph sequence until loss of fine pointing by the rocket pointing system. We have the option of continuing the filter sequence, or of switching to the post flight sequence. If we choose not to switch at this time, then we will go to the post flight sequence upon loss of fine pointing by the rocket pointing system.

POST FLIGHT PHASE:

This is the spectrograph observing sequence that was previously defined by Dr. Dame during our July / Aug. observing run. It consists of observations with the echelle of a 1 x 1 arc minute field with 30 sec

repetition rate using the CCD array for Ca K line profiles.

ORGANIZATION AND COMMUNICATIONS PROTOCOL

In order to avoid potential misunderstandings and possible conflicts, we recognize the importance of defining and adhering to a clear line of communication and authority between the rocket launch operation, and the ground based observing team. The rocket launch team is under the direction of Dr. M. Bruner, who is the NASA Principal Investigator on the rocket program. Other rocket team members include Dr. W. A. Brown, Dr. L. Dame, Mr. R. Caravalho, and Mr. M. Decaudin. M. Bruner will serve as the prime contact for all communications with the rocket team. We propose that Dr. J. Zirker serve as our prime contact with the Sacramento Peak observing staff. It is understood that all communications that affect the observing program of either group will be routed through these two individuals. We will be pleased to provide assistance with the necessary setup of the equipment, and can provide an assistant observer to be at the Peak on the day of launch. The assistant observer would be under the direction of Dr. Zirker for the duration of the flight operation.

DATA ANALYSIS, INTERPRETATION, AND PUBLICATION

Participation of Sacramento Peak staff members in the analysis, interpretation and publication of the data resulting from our observing run will be welcomed and is actively solicited. We expect that Sac Peak staff members will share co-authorship in the resulting publications as appropriate, and that the Sac Peak effort will be fully acknowledged. We will probably need some assistance with microdensitometry of the film, and would like to use the automated equipment that you have prepared for this purpose. We can probably supply a trainable warm body (M. Bruner) to help operate the equipment. We sincerely hope that these arrangements will be satisfactory to you, and look forward to a very productive collaboration.

REFERENCES

Bonnet, R.M., L.W. Acton, W.A. Brown, M. Decaudin, and B. Foing: 1980, Astron. Astrophys. 111, 125.

Liu, S.Y., N.R. Sheeley, Jr., and E.v.P. Smith: 1972, Solar Phys. 23.

Liu, S.Y.: 1972, 'Fine Structure in the Solar Chromosphere', Ph.D. Thesis, Univ of Maryland

Sivaraman, K.R., and W.C. Livingston: 1982, Solar Physics, 80, 227.

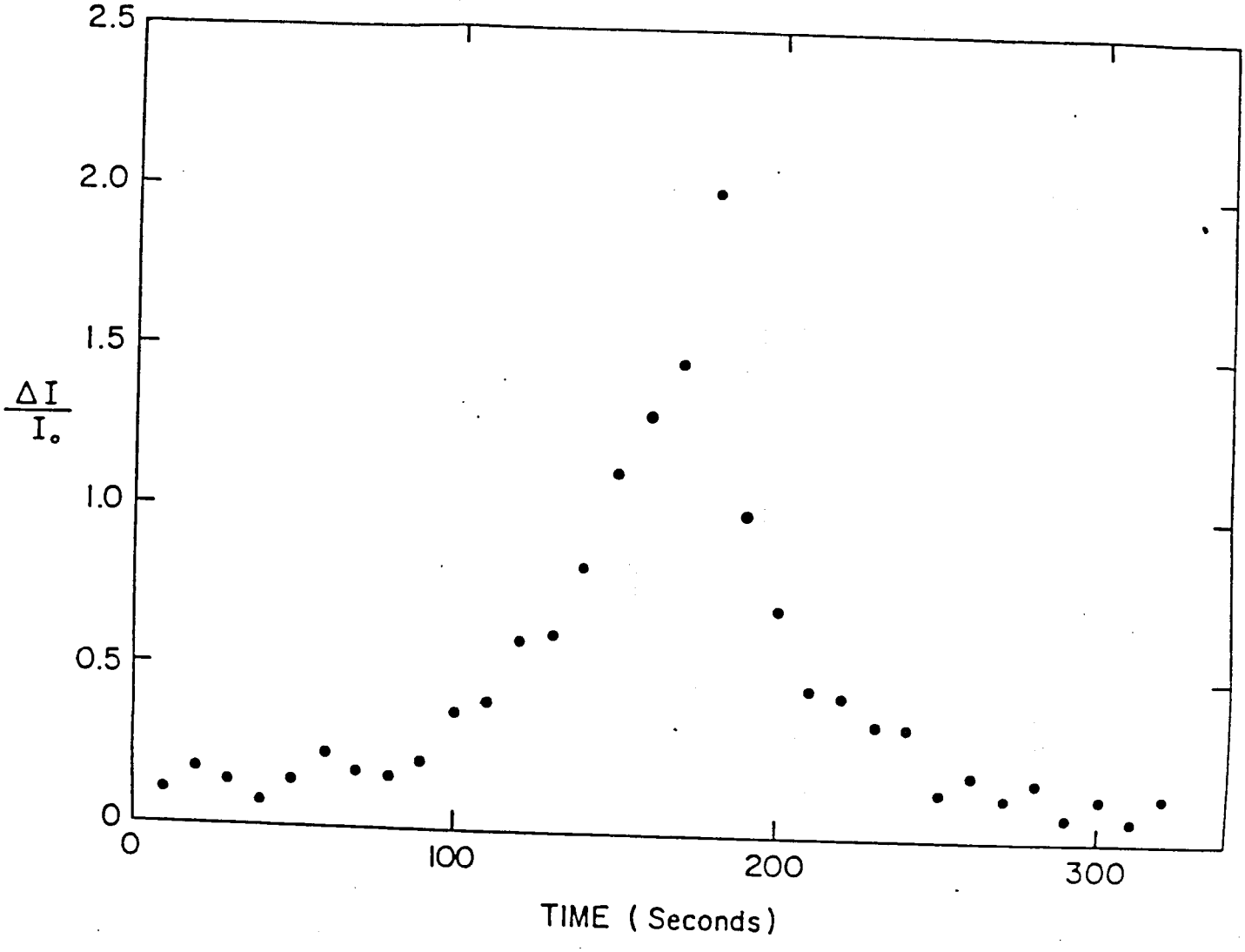

Figure 1

Reproduced from Liu, (1972)

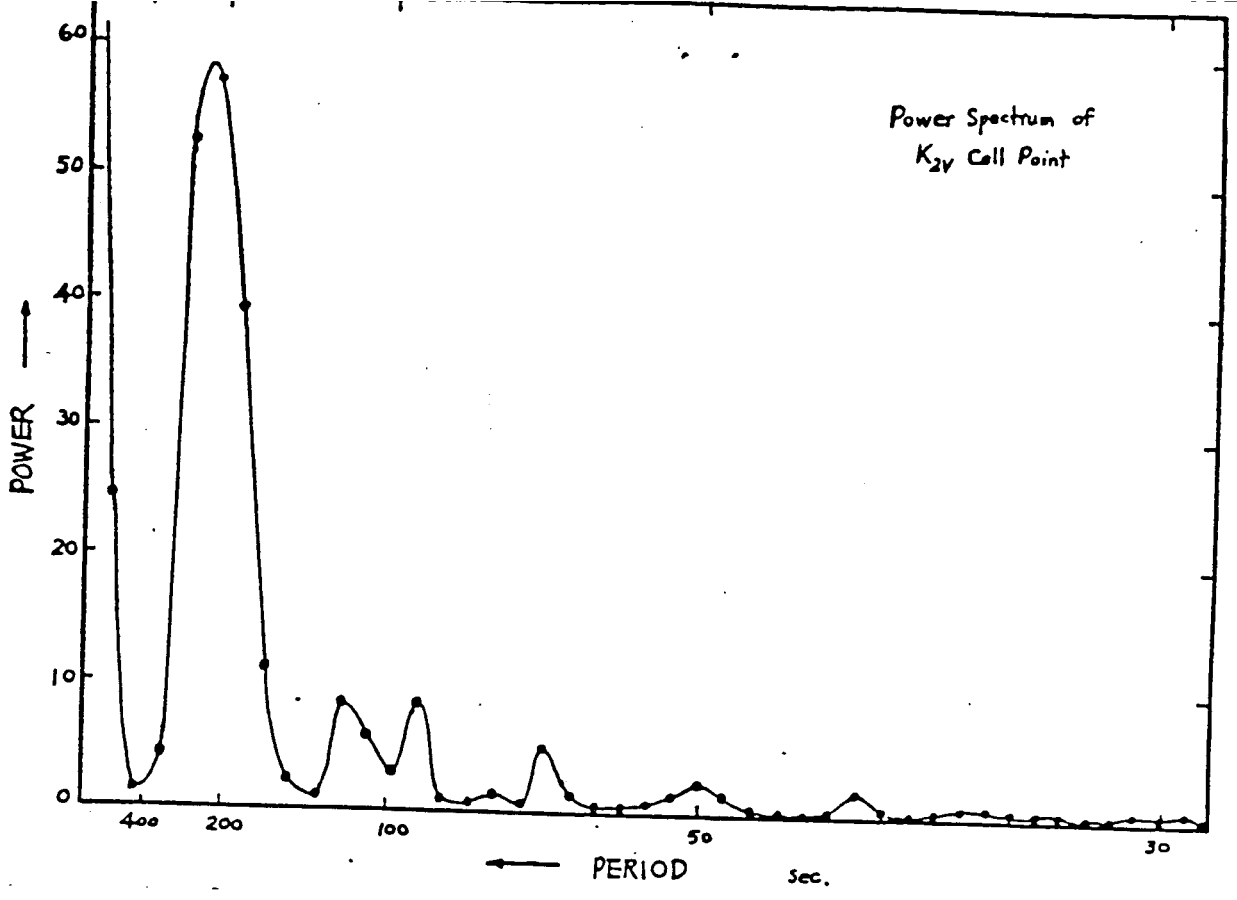

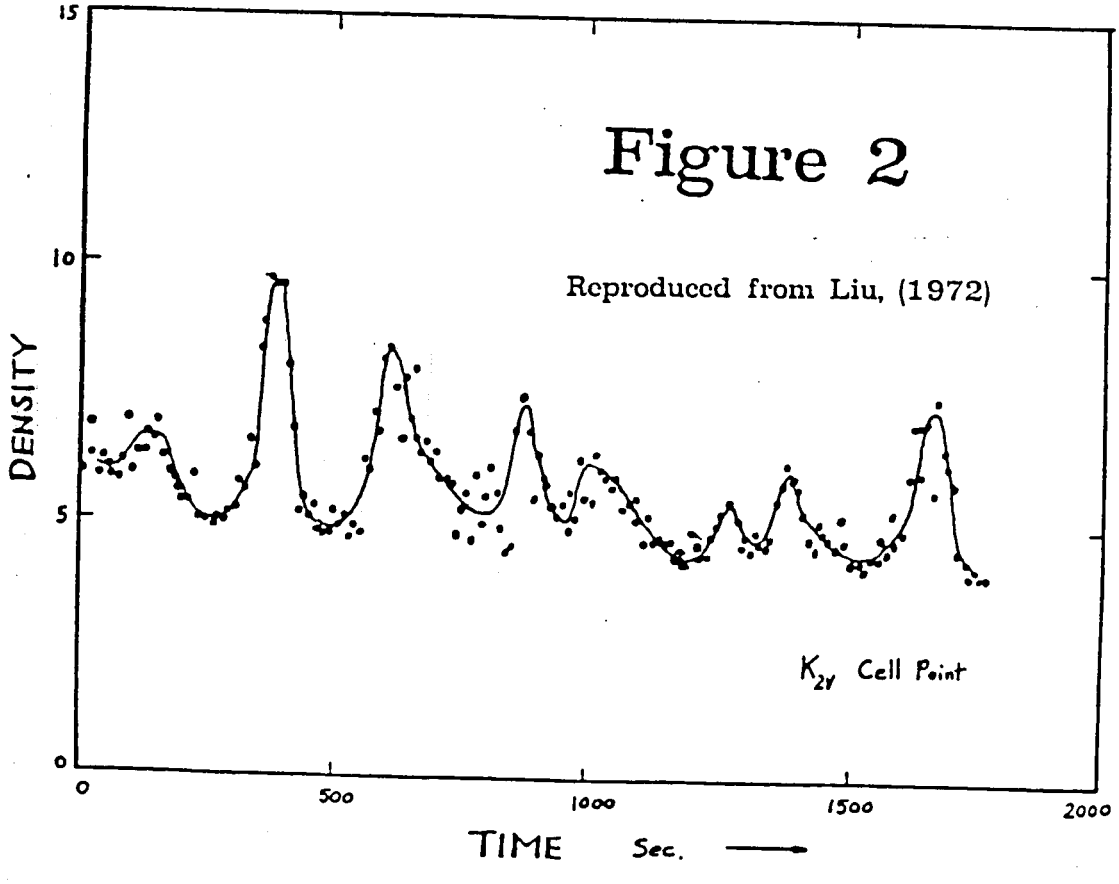

Figure 2

APPENDIX 4

SPARTAN Experimenter's Preliminary Data Package

REV A JULY 14, 1985

SPARTAN
EXPERIMENTER'S PRELIMINARY DATA PACKAGE
LMSC-D088449

1.0 OVERVIEW

1.1 SCOPE This document will present supplementary information on the High Resolution Solar Study payload described in Lockheed proposal number LMSC-D088449, dated 2 July, 1984. The scientific objectives were described in detail in the proposal, and will be treated only very briefly here. Our approaches to the hardware design, however, have evolved considerably in the past year in ways that we believe will both improve performance, and lower the costs of the hardware. These areas will be discussed in the material to follow.

1.2 OBJECTIVES The general objectives of the science program are studies of the physical conditions in the atmosphere of the sun, using techniques of high resolution soft X-ray spectroscopy, moderate to high resolution soft X-ray imagery, and high resolution ultraviolet imagery. The UV and X-ray data will be related to other known solar phenomena by means of visible light images made in the H alpha and Ca II k lines. The payload is seen as an evolving set of co-ordinated instruments used in an integrated observing program. We expect that because of limitations on the level of funds available to us, not all of the instruments described in the proposal will be ready for the first flight of the system. The full complement of instruments is listed in Table I, reproduced here from the proposal.

1.3 REVISIONS Major areas of revision from the proposal include an improved approach to the structural system which we call SPOTS; the use of a commercially available microcomputer system as the basis for our electrical controls; and a decision to use Nikon or equivalent cameras in lieu of specialty cameras for the visible light imaging systems, and for the soft X-ray imaging system.

2.0 THE SPARTAN OPTICAL TABLE SYSTEM (SPOTS)

2.1 APPROACH The SPOTS sturcture is a bolted assembly, consisting of a pair of parallel rectangular plates separated by two aluminum H beams, as shown in Figure I. Optical components of the UV and soft X-ray imaging systems will be mounted on the upper plate, which serves as an optical table. The components of the X-ray spectrographs will be mounted on the web of one of the H beams, while the two visible imaging systems will be mounted on the other H beam. Additional mounting surface is available on the lower plate for the components of instruments that may be incorporated in the future. It will be seen that the structure consists,in effect, of two optical tables, separated by two optical benches. This configuration is extremely stiff when

assembled, but can be separated into four major subassemblies for ready access to the optical components.

2.2 DIMENSIONS The lower table of SPOTS is 24 in. wide by TBD in. long (aprox 110 in.). The upper table is 22 in. wide, and has the same length as the lower table. The lower table is 1 inch thick, and the upper table 0.75 in. thick. The nominal size of the H beams is 9 in. between the outer flange faces, and the face widths are 5 in. Their lengths are the same as those of the tables (aprox. 110 in.).

2.3 OPTICAL TABLE CONSTRUCTION Each optical table is a composite system, consisting of an aluminum foam core and two aluminum face sheets which are bonded to the core by dip brazing. Solid aluminum slugs are insterted in the core prior to face sheet bonding wherever tapped mounting holes are required, and in locations where large compressive loads must be supported. Mounting bolts for each table pass through both face sheets, so that all parts of the table are completely captured, in the event of a failure of the face sheet bonding.

2.4 H BEAM CONSTRUCTION The H beams are extrusions of 50 series aluminum alloy, heat treated to the O condition. Webs and flanges are 0.25 in. thick, and the outer flange surfaces are finish machined for flatness and parallelism.

2.5 ATTACHMENT TO SPARTAN The SPOTS structure is attached to the SPARTAN service module by a series of bolts passing through the lower optical table and the lower flanges of the two H beams. Attachment is to this surface only, so that the special mounting bracket mentioned in our proposal is no longer required.

3.0 THERMAL CONTROL SYSTEM

3.0 APPROACH The thermal control approach is to thermally isolate the instrument compartment from the environment through the use of conductive and radiative isolation and to use small heaters, radiatively coupled to the SPOTS structure to maintain the system at its operating temperature. The design has not been subjected to detailed analysis, and GSFC support for this analysis is requested.

3.1 THERMAL ISOLATION Thermal isolation from the SPARTAN structure will be required. Conductive isolation may be provided by inserting insulating spacers between the lower optical table and the SPARTAN service module and by using titanium bolts for the mechanical attachment. Multilayer insulation between the SPOTS and the SPARTAN service module will be required to provide radiative isolation. Multilayer insulation is also required around the main instrument module of the SPARTAN payload. We request that the required multilayer insulation be government furnished.

3.2 HEATER SYSTEM The thermal control heaters are to be mounted on a light weight envelope that completely surrounds the

instrument compartment and the SPOTS structure. Our current concept calls for this envelope to be supported from a light weight skeleton that is attached to the SPOTS structure. The envelope / heater assembly acts as an constant temperature cavity in which the instrument assembly operates. The multilayer insulation blanket reuqired for thermal isolation from SPARTAN and the outer radiation environment surrounds the entire instrument compartment, including the thermal control envelope.

4.0 THE SPARTAN INSTRUMENT CONTROL SYSTEM

4.1 APPROACH The instrument control system is based on the MA2000 series macrocomponents, a commercially available microcomputer system manufactured by National Semiconductor. The computer system consists of a series of modules connected by a common bus that includes a Z-80 compatible microprocessor, memory, timers, and I/O modules. It was designed for control and data acquisition use in a fairly severe mechanical environment such as found in industrial applications. Control algorithms will be implemented in the MA2000 system in FORTH. The computer will furnish all necessary digital control lines via open collector outputs and will monitor digital status via two 8 bit parallel input ports. Isolation and high current drivers are the only required external electronics. The system will be driven by the SPARTAN computer via a bidirectional interface using an industry standard protocol.

4.1 BLOCK DIAGRAM A block diagram of the instrument system is shown in Figure II. There are four major components to the system, The MA2000 computer, the isolation / drive module, the power converter, and the instrument / mechanism subsystem. Interfaces to SPARTAN include the computer interface on the left, and the tape recorder and PCM interfaces on the right. Interconnects between the MA2000 and the instrument subsystem are shown by arrows on the diagram indicating the direction of information flow, and the number of bits involved. The top line in the drawing, for instance, shows that two open collector outputs are required to actuate the door over the Lyman alpha telescope. One status bit indicating the door position is returned to the MA2000. The isolation drive module simply passes the signals through, adding buffering or increased current drive capacity as needed by each particular device.

4.2 SPARTAN / MA2000 INTERFACE The MA2000 as implemented in our instrument package, requires an RS232 serial interface for its operation. This choice is dictated by severe budget constraints on the level of effort available to us, making it mandatory that our hardware and software efforts be held to an absolute minimum, with maximum use of off-the-shelf hardware and operating system software. Use of the RS232 industry standard interface and protocol os a very powerful way of meeting this requirement. It not only permits us to simply buy our interface hardware, it also allows to use a cheap and readily available computer terminal as our ground supoort equipment. Equally

important, it allows us to develop our control algorithms with a minimum of programming effort, since most of the required software is already complete in the operating system that is furnished with the computer.

The RS232 interface can be easily implemented in the current SPARTAN hardware design by adding an appropriate remote interface module that makes the necessary serial to parallel conversions. Lockheed would be pleased to furnish a quote on the design and construction of the remote interface module, but we are unable to supply it under the very limited budged available to us in the instrument program.

Control of our instrument via the RS232 interface is accomplished by transmitting the ASCII characters required to invoke the FORTH words assigned to each major observing mode. Confirmation of proper operation of the instrument is signified by the OK response that the FORTH system returns at the completion of successful program execution. All digital status developed by the instrument hardware will be available in the MA2000, and may be interrogated by invoking an appropriate FORTH word.

4.3 PCM INTERFACE Signals presented to the SPARTAN PCM interface will be of two types. Analog signals will include a number of temperature monitors, voltage levels, and current monitors; the exact number and their placements to be determined. The signals from the radiometer detectors in the X-ray spectrograph will be streams of pulses from two photomultipliers. These streams will need to be captured by pulse counters in the PCM system and periodically read out into the normal SPARTAN data handling system. The data rates are relatively low, and will not present a major data handling problem. These pulse streams are the data needed by the SPARTAN computer to execute the target acquisition sequences discussed in our proposal.

4.4 TAPE RECORDER INTERFACE The CCD system of the ultraviolet filtergraph will generate a very substantial data set, as indicated in our proposal. We have requested that a MARS tape recorder be dedicated to this detector if at all possible. The details of this interface are TBD at this time, and interface design consultation is requested from GSFC to clarify the approach.

TABLE 1
SPARTAN
INSTRUMENT COMPLEMENT

1. X-RAY SPECTROGRAPH

• Spectral Range:	20 to 120 A 1st order 10 to 25 A 2nd order
• Spectral Resolution:	20 mA
• Pixel Size:	2 by 30 arc seconds
• Primary Detector:	Film (Kodak 101-07)
• Secondary Detectors at Central Image:	
8-15 and 44-60A	Spiraltron photomultiplier plus Aluminized Mylar window
1430-1680A	EMR 510G photomultiplier (CsI)

2. HRUVIS - HIGH RESOLUTION UV IMAGING SYSTEM

Lyman Alpha Camera

• Spectral interval	1215 +/- 40 Angstroms
• Telescope	Extended TRC Cassegrain
focal length	4 meters
field	10 x 18 arc min
resolution	0.5 arcsec
• Filter	Interference filter Mag F substrate
• Detector	Film (Kodak 101-01) 1200 exposures exposure time: less than 1 second

Narrow Band UV Photoelectric Imager

• Spectral interval	1550 +/- 4 Angstroms 1580 +/- 4 Angstroms
• Telescope	20 cm diam Cassegrain
• focal length	16 meters
• field	2.8 x 2.8 arc minutes
• resolution	0.5 arc sec
• Filter	Tunable Fabry-Perot
• Detector	CCD behind microchannel plate 512x512 pixels of 20 microns exposure time: 1/4-1/2 sec

3. VISIBLE BAND IMAGING SYSTEM

H-Alpha telescope

• Range Selection:	Fabry-Perot plus interference filter
• Spectral Bandpass:	0.75 A
• Spatial Resolution:	1 arc seconds
• Detector:	Film (KodakSO-392)

K-line telescope

- ~~shares film camera with above~~
- separate telescope--new filter for Ca II 3939 A

4. X-RAY IMAGING SYSTEM

• Spectral Range:	peak wavelengths at 44,33,95
• Bandpass Selection:	Multilayer Mirror
• Spectral Resolution:	2 to 4 % of peak wavelength
• Detector:	Film (Kodak 101-01)

5. FLAT FIELD X-RAY SPECTROGRAPH

• Spectral Range	30-45 A
• Spectral resolution	20 mA
• Spatial Resolution	2 arc sec
• Field of view	1 arc minute

FIGURE I
SPARTAN OPTICAL TABLE SYSTEM (SPOTS)

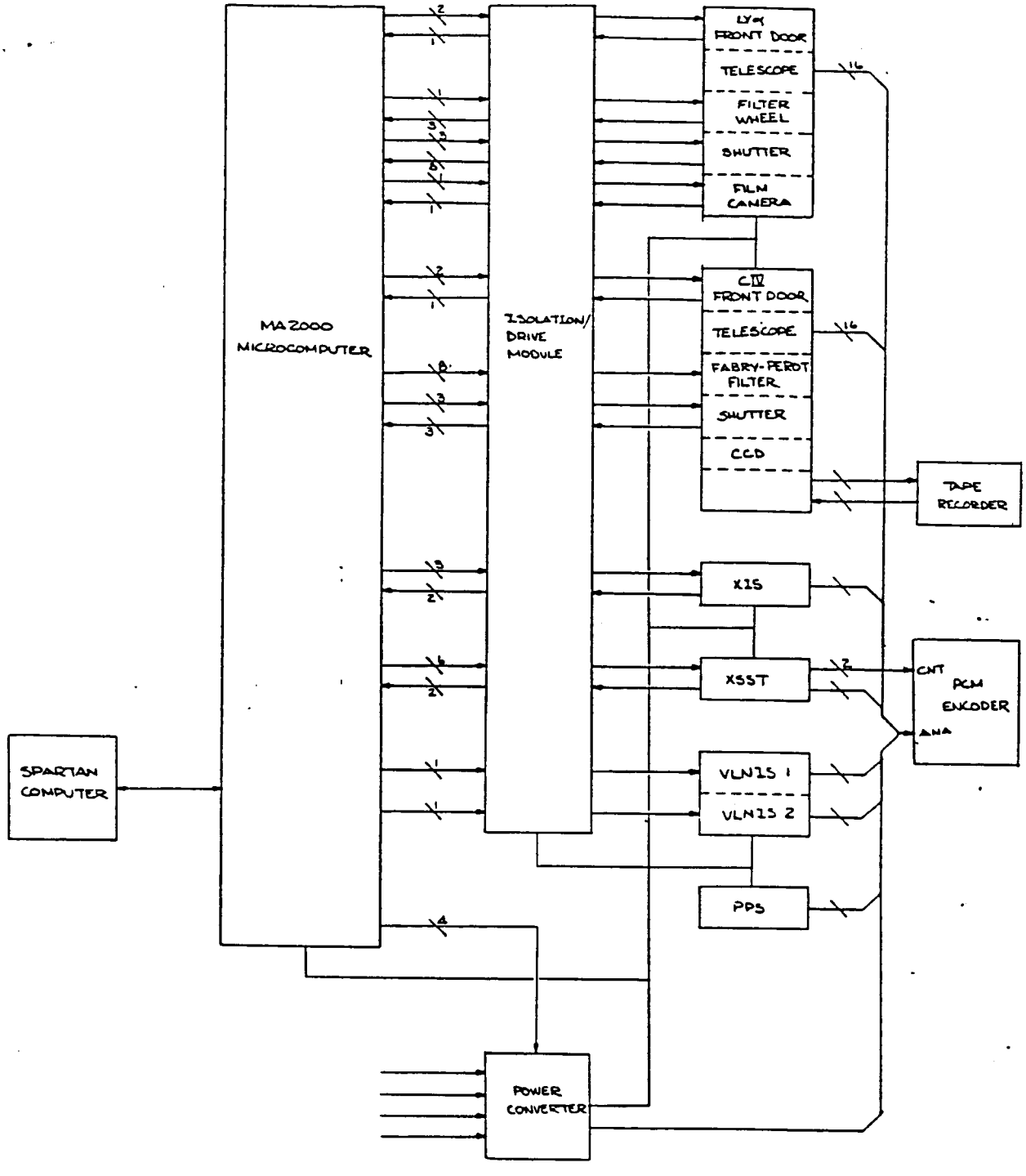

FIGURE II

LPARL SPARTAN SYSTEM
BLOCK DIAGRAM

R. CARVALHO
7-19-85

APPENDIX 5

Preliminary Design Concept for the Rocket / Spartan Payload

REVISIONS				
ZONE	REV	DESCRIPTION	DATE	APVD

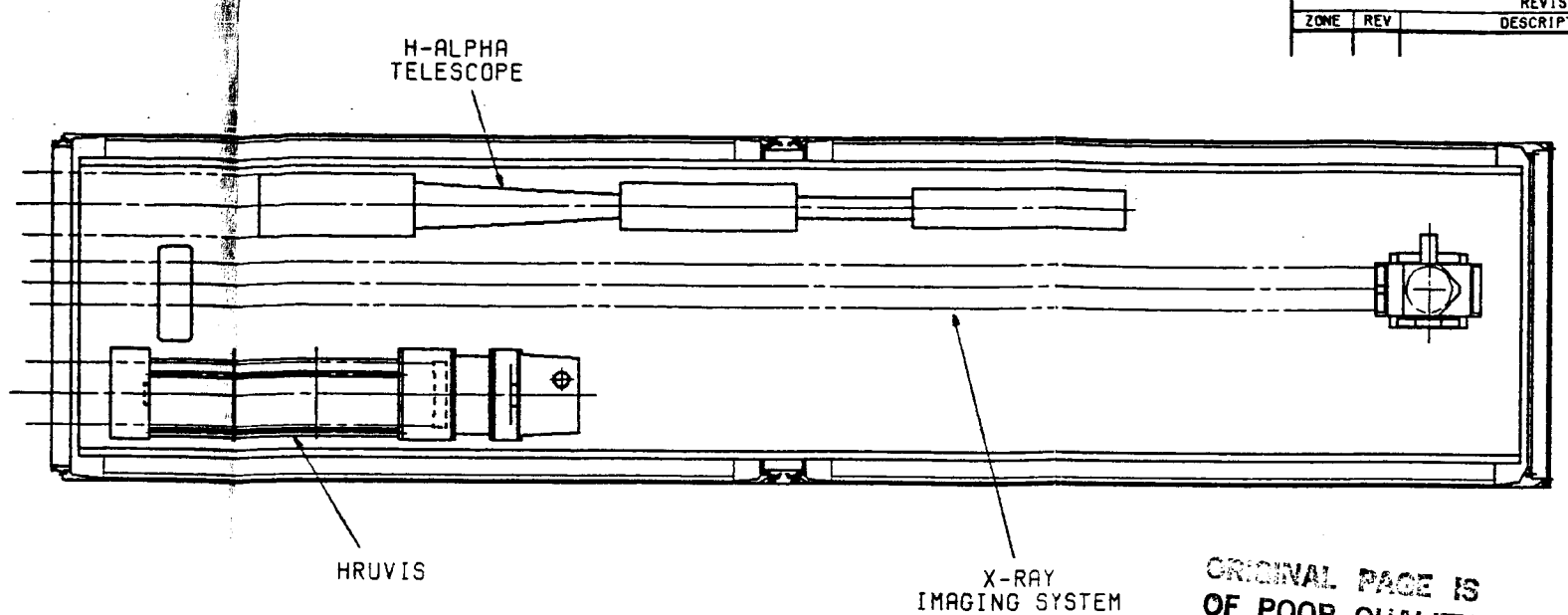

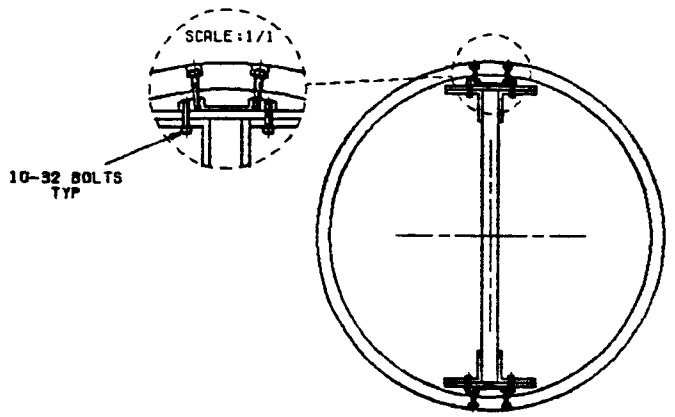

SECTION A-A

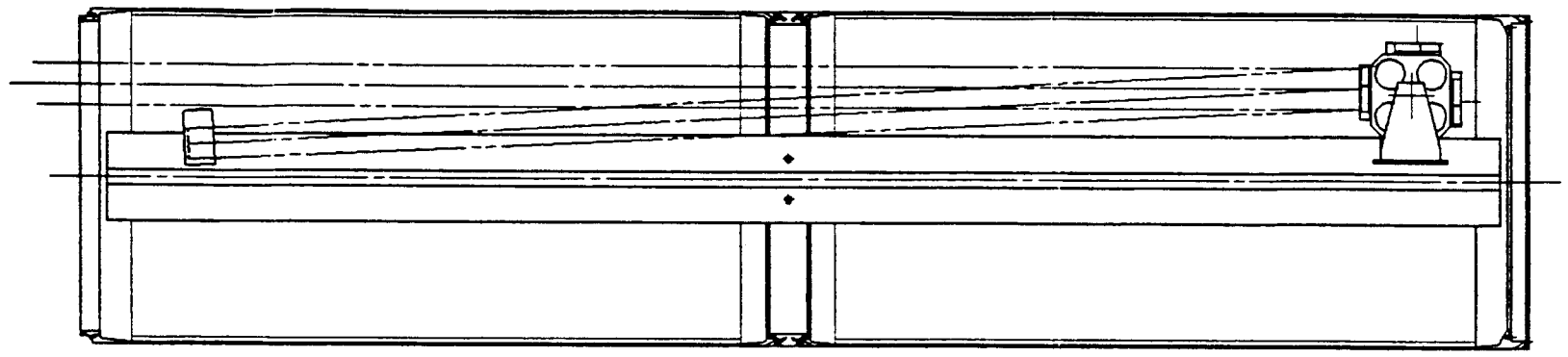

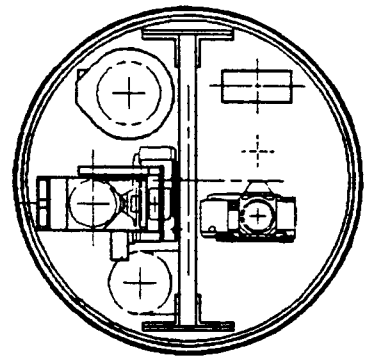

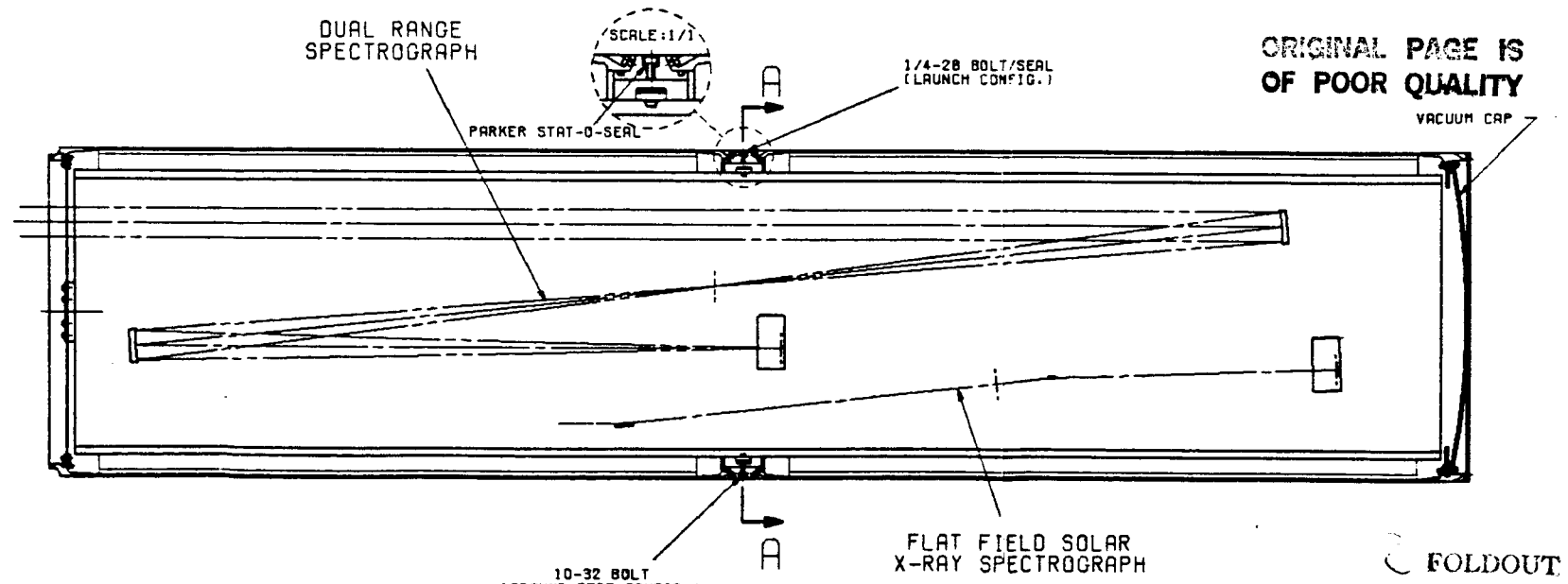

FOLDOUT FRAME

FOLDOUT FRAME

QTY REQD	FSCM	PART OR IDENTIFYING NO	NOMENCLATURE OR DESCRIPTION	MATERIAL DESCRIPTION OR NOTE	MATERIAL SPECIFICATION	ZONE	ITEM NO

PARTS LIST

UNLESS OTHERWISE SPECIFIED DIM. ARE IN INCHES. TOLERANCES ON:
FRACTIONS = ± 1/16
DECIMALS: .X = ± .1
.XX = ± .03
.XXX = ± .010
ANGLES = ± 2 DEG.

NEXT ASSY | USED ON | APPLICATION

DATE 30 JUNE 87
DWN D.STUBBS
APVD
APVD
ENGRG
CHKR
APVD
CONTR
CCA/CI
APVD

LOCKHEED MISSILES & SPACE COMPANY, INC.
SUNNYVALE, CALIFORNIA

SPARTAN
OPTICAL TABLE
LAYOUT

SIZE E | FSCM 65113 | DRAWING NO SPARTAN 0038 | REV B

SCALE 1/4 | SHT 1 OF 1

NASA

REPORT DOCUMENTATION PAGE
(IN LIEU OF NASA FORM 1626)

1. REPORT NO.	2. GOVERNMENT ACCESSION NO.	3. RECIPIENT'S CATALOG NO.
DR-01		

4. TITLE AND SUBTITLE	5. REPORT DATE
VERY HIGH RESOLUTION UV AND X-RAY SPECTROSCOPY AND IMAGERY OF SOLAR ACTIVE REGIONS FINAL REPORT	June 30, 1987
	6. PERFORMING ORGANIZATION CODE

7. AUTHOR(S)	8. PERFORMING ORGANIZATION REPORT NO.
M. Bruner W. A. Brown B. M. Haisch	D068438
	10. WORK UNIT NO.

9. PERFORMING ORGANIZATION NAME AND ADDRESS	11. CONTRACT OR GRANT NO.
Lockheed Palo Alto Research Labs Space Sciences Laboratory O/91-20 3251 Hanover Street , Palo Alto Ca. 94304	NAS5 - 25727

12. SPONSORING AGENCY NAME AND ADDRESS	13. TYPE OF REPORT AND PERIOD COVERED
NASA Goddard Space Flight Center Wallops Flight Facility Wallops Island, VA 23337	Final Report 25 Sep 79 thru 30 Jun 87
	14. SPONSORING AGENCY CODE GSFC 244.3/603

15. SUPPLEMENTARY NOTES

16. ABSTRACT This report describes a scientific investigation of the physics of the solar atmosphere, using the techniques of high resolution soft X-ray spectroscopy and high resolution UV imagery. The experiments were conducted during a series of three sounding rocket flights. All three flights yielded excellent images in the UV, showing unprecedented spatial resolution. The second flight recorded the X-ray spectrum of a solar flare, and the third that of an active region. A normal incidence multi-layer mirror was used during the third flight to make the first astronomical X-ray observations using this new technique.

17. KEY WORDS (SUGGESTED BY AUTHOR(S))	18. DISTRIBUTION STATEMENT
X-Ray, UV, Spectra, Space Science, Solar Physics Solar Flares, Multilayer Mirrors	"Unclassified - unlimited"

19. SECURITY CLASSIF. (OF THIS REPORT)	20. SECURITY CLASSIF. (OF THIS PAGE)	21. NO OF PAGES	22. PRICE
None	None	73	

For sale by the Superintendent of Documents, U.S. Government Printing Office, Washington, D.C. 20402-0001